EXPERIMENTAL INVESTIGATION OF HYBRID FLUID OSCILLATORY MOTION AND HEAT TRANSFER IN OSCILLATING HEAT PIPES

A Thesis

Presented to

the Faculty of the Graduate School

at the University of Missouri – Columbia

In Partial Fulfillment

of the Requirements for the Degree

Master of Science

---

by

ADALBERTO AVILES

Dr. Hongbin Ma, Advisor and Thesis Supervisor

MAY 2022

The undersigned, appointed by the Dean of the Graduate School, have examined the thesis entitled

EXPERIMENTAL INVESTIGATION OF HYBRID FLUID OSCILLATORY MOTION AND HEAT TRANSFER IN OSCILLATING HEAT PIPES

presented by Adalberto Aviles,

a candidate for the degree of Master of Science in Mechanical Engineering,

and hereby certify that, in their opinion, it is worthy of acceptance.

_____

Dr. Hongbin Ma

_____

Dr. Matthew R. Maschmann

_____

Dr. Yangchuan Xing

Acknowledgments

The work presented in this paper was funded by the Office of Naval Research, under the direction of Dr. Mark Spector.

Thank you, Dr. Ma, my advisor, and research sponsor, for the opportunity to further pursue a passion of mine, as well as helping me be the first person in my family to achieve a Master of Science degree. I am forever grateful for being patient and understanding, as well as for the wise guidance throughout my education that has helped me grow not only as a professional but as a person.

Dr. Ma

Alberto Aviles

Dionicia Medrano

Michael Merwin

ThermAvant International, LLC.

ThermAvant Technologies, LLC.

Susan Liu

Laith Ishmael

Tingting Hao

Pengtao Wang

Mark Owoola

Table of Contents

List of Figures

List of Tables

Nomenclature

A	cross-sectional area
c	specific heat
D	tube diameter
f	friction factor
G	mass flux
h	heat transfer coefficient
h_{lv}	latent heat
HF	Hybrid Fluid
k	thermal conductivity
K	curvature
L	length
m	mass
OHP	Oscillating Heat Pipe
p	pressure
Pr	Prandtl number
q''	heat flux
r	radius
R	gas constant
Re	Reynolds number
s	location
S	suppression factor
T	temperature
t	time
u	oscillation velocity
x	coordinate; quality
X	Martinelli parameter
y	mass fraction
Y	mole fraction
z	direction

Greek

δ	film thickness
ϕ	filling ratio
κ	stiffness
ρ	density
$\overline{\rho}$	average density
μ	viscosity
ω	frequency
σ	surface tension
ζ	damping ratio

Subscripts

c	condenser; condensing; capillary

e	evaporator; evaporating	min	minimum
h	hydraulic	o	outer
i	inner	*p*	pressure
l	liquid	sat	saturated
mac	macro	tp	two phase
max	maximum	*v*	vapor
mic	micro	*w*	wall

Abstract

Mathematical models predicting the oscillatory motions as well as the heat transfer effects of hybrid fluids (HF) in an oscillating heat pipe (OHP) are simulated. The models consider the vapor bubble as the gas spring for the oscillatory motions including effects of operating temperature, vapor bulk modulus, and temperature difference between the evaporator and the condenser. Using the theoretical hybrid fluid oscillatory motions from the developed models, heat transfer models showing the theoretical temperature differences in the evaporator and the condenser are developed including the effects of forced convection heat transfer due to the oscillating motion, the confined evaporating heat transfer in the evaporating section, and the thin film condensation heat transfer in the condensing section. Furthermore, an experimental investigation was conducted on a copper hybrid fluid oscillating heat pipe (HFOHP) with six turns. It is observed that the analytical models resemble and follow the same trends as the experimental data gathered. Results show that the changes in the working fluid's thermal properties due to the addition of gallium significantly helps to increase the heat transfer performance of a water OHP and helps provide a better understanding of HFOHP optimization for applications in high-powered systems.

Chapter I. Introduction

Today's current rapid technological growth has established thermal management as a major engineering obstacle. In order to meet current consumer and military needs, modern technologies are requiring higher levels of efficient and consistent thermal energy dissipation. Following in accordance with Moore's Law, computer chip technology continues to advance and their size decrease, with heat flux levels rapidly increasing. For example, some laser diode applications reach heat flux levels of up to 500 W/cm^2. With heat flux levels this high, traditional heat transport devices including heat pipes are no longer adequate to maintain the low temperatures required for safe use of these modern computers, because the heat transfer limitation of conventional heat pipes prevents these devices from being utilized. Heat pipes, which utilize phase change heat transfer, were developed to meet the increased demands for better heat dissipation. Heat pipes provide a way to passively remove thermal energy from a source in a quick and efficient manner. Heat pipes are an energy transport device that effectively utilizes phase change of a fluid to transport heat. Heat pipes are attached to a heat source which is intended to be cooled. The heat conducts through the wall of the heat pipe and reaches the working fluid inside. The liquid vaporizes and absorbs the heat through phase change. The vapor then flows along the pipe to the colder condenser region. The vapor releases its latent heat when it condenses back into a liquid. Latent heat of vaporization is the energy required to cause a liquid to transition to vapor. Because pure working fluids exist inside the heat pipe, the phase change can take place at any temperature between the freezing point and critical temperature.

An oscillating heat pipe (OHP) is a new heat transfer device that utilizes two-phases and relies on oscillating flow of liquid plugs and vapor bubbles in order to increase heat transport capabilities to higher levels than can be obtained by a conventional heat pipe. The OHP is

comprised of a long capillary tube with many turns. The tube is partially filled with a working fluid such as water, acetone, etc. The pressure difference across the liquid-vapor interface due to the small radii of OHP tubes/channels and liquid surface tension can separate into liquid slugs and vapor bubbles in the capillary tubes/channels of OHPs. The working fluid is heated up in the evaporator, and a small portion is vaporized. This creates vapor pressure which is a driving force for moving the heated liquid to the condenser section. The condenser then cools the liquid allowing the vapor to condense. Because the pressure inside is directly related to the temperature, a higher temperature in the evaporator results in a higher pressure and a lower temperature in the condenser produces a lower pressure. This pressure difference between the evaporator and condenser plus the unbalanced design of OHP with many turns produces the oscillating motion of a train of liquid plugs and vapor bubbles. While the phase change heat transfer by the latent heat produces the thermally excited oscillating motion, most of heat is transferred from the evaporator to the condenser is by the sensible heat transfer. Sensible heat is the energy absorbed or released due to the heat capacity of a working fluid when a temperature change occurs. While a small portion of thermal energy transfer comes from the vaporization and condensation of the fluid, i.e., latent heat, the phase change heat transfer produces the key driving force for the oscillating motion of a train of liquid slugs and vapor bubbles throughout the tubes or microchannels in an OHP. Because the OHP is thermally driven, the OHP can transport heat long distances and can operate in many conditions such as zero gravity or 10-g gravity. This is in contrast to traditional heat pipes that rely on the capillary pressure only. The increased heat transfer capabilities are mainly attributed to: (1) The working fluid does not travel through a wick, resulting in a low pressure drop of the working fluid. (2) There is no interference between the vapor flow and liquid flow because they are moving in the same direction. (3) The vapor

plugs can be formed within the OHP because of the small diameter of the OHP. (4) The heat added on the evaporating area is distributed by the forced convection due to the oscillating motion along with the phase-change heat transfer [1-6]. In addition, OHP heat transfer performance does not depend on gravity and can be fabricated into any shape. Currently, OHPs have been utilized in many applications such as naval GBIT devices, aerospace lightweight heat spreaders, and satellite cooling systems.

Extensive experimental investigations [1–6] and theoretical analysis [7–15] have been conducted and show that there exist oscillating or/and circulating motions in an OHP, which depend on working fluids [2–4,10], tilt angles [5–7], dimensions [2,6,9,10,13], filling ratio [5,9,14], number of turns [2,4,13], and heat flux levels [2,4,7,14]. These investigations have provided an insight into the mechanisms of oscillating motions occurring in the OHP. Furthermore, the primary factors affecting the heat transport capability have been studied, which show that OHP heat transport capabilities are driven by the effects of the forced convection heat transfer due to the oscillating motion, the confined evaporating heat transfer in the evaporating section, and the thin film condensation in the condensing section [16].

Liquid metals have been extensively studied in heat transfer applications and it has been observed that heat transfer performance is significantly enhanced by using a liquid metal working fluid [17]. The best candidates of liquid metal suitable for heat transfer management working under 100 °C are gallium and its alloys due to their low melting points [17]. Room temperature liquid metals including gallium or its alloys such as EGaIn (75% gallium and 25% indium by weight) and galinstan (68.5% gallium, 21.5% indium, and 10% tin by weight) own many intriguing properties. Gallium and its alloy galinstan are non-toxic room temperature liquid metals with melting points of 29.8 and −19 °C, respectively. Furthermore, gallium has a large

surface tension, a high thermal conductivity, and a high electrical conductivity. The thermal conductivity of gallium is 24 W/m·K, which is approximately 41 times higher than that of water, while the dynamic viscosity is only twice that of water [17]. Gallium is also quite compatible with other metals in certain temperature environments, including chromium, copper, and tungsten, which can be used with gallium at temperatures below 600 °C. Due to these merits, gallium, and its alloy galinstan can potentially be used in next generation cooling devices.

In this investigation, a fundamental understanding of the oscillating flow and heat transfer of hybrid fluids (HFs) in a OHP is developed. A hybrid fluid is defined as a mixture of two different fluids, usually a liquid metal and water. In this investigation, a hybrid fluid of gallium and water is used. Building upon the work done by previous experimental investigations and results, mathematical models predicting the oscillatory motions as well as the heat transfer effects of a hybrid fluid oscillating heat pipe (HFOHP) are simulated using MATLAB, which include the effects of the forced convection heat transfer due to the oscillating motion, the thin film evaporating heat transfer in the evaporating section, and the thin film condensation in the condensing section. Experimental investigations are then conducted in order to compare and analyze the developed analytical models to the experimental investigations conducted. Results of the combined analytical and experimental investigation will help to understand the mechanisms of integrated heat transfer enhancement from oscillating motion enhanced by thin film evolution and evaporation of water, condensation on a liquid metal surface, and high thermal conductivity of room-temperature liquid metal.

Chapter II. Theoretical Analysis

2.1 Mathematical Modeling

An OHP consists of an evaporating section, an adiabatic section, and a condensing section as shown in Fig. 2.1.

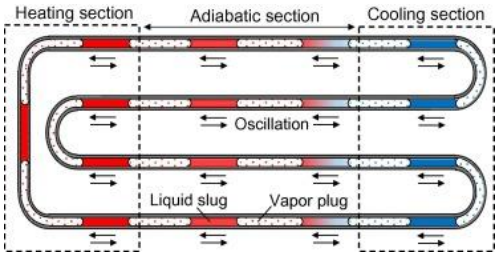

Fig. 2.1 Schematic of an OHP

2.1.1 Oscillatory Motion in an Oscillating Heat Pipe

For a typical OHP, the hydraulic diameter must relatively small so that the surface tension can make liquid plugs separated by vapor bubbles. The vapor bubbles in the OHP can be seen as the 'springs' for the oscillating motion generated in the system. In order to greatly reduce the extensive computing power and time required from the theoretical models, as well as to greatly reduce the complexity of equations, it is assumed that all liquid plugs behave as one liquid plug and all vapor bubbles as one vapor bubble. When heat is added to the evaporating section, the heat will be transferred through the wall and reach the working fluid. As it does, the saturated liquid will be vaporized into saturated vapor. If the vapor temperature in the evaporator, T_e, is known, the vapor pressure in the evaporating section, p_e, can be determined by the Clapeyron equation

$$p_e = p_0 e^{\left[\frac{h_{lv}(T_e - T_0)}{RT_eT_0}\right]} \tag{2.1.1}$$

Following the same approach, the vapor pressure, p_c, in the condenser section can be determined if the vapor temperature in the condensing section, T_c, is given. The pressure difference between the evaporating section and the condensing section can thus be found by

$$\Delta p = p_e - p_c = p_c \left[e^{\left(\frac{h_{lv}(T_e - T_c)}{RT_eT_c} \right)} - 1 \right] \tag{2.1.2}$$

Utilizing a Taylor series and neglecting high-order terms, the equation above can be simplified as

$$\Delta p = \Delta T \left(\frac{h_{lv}\rho_{v,c}}{T_c} \right) \tag{2.1.3}$$

where

$$\Delta T = \left(\frac{\Delta T_{\max} - \Delta T_{\min}}{2} \right) \left[1 + \cos(\omega t) \right] \tag{2.1.4}$$

for an oscillating system. Substituting, the driving force to cause the oscillating motion can be found as

$$F_D = \Delta pA = \left(\frac{Ah_{lv}\rho_{v,c}}{T_c} \right) \left(\frac{\Delta T_{\max} - \Delta T_{\min}}{2} \right) \left[1 + \cos(\omega t) \right] \tag{2.1.5}$$

where A is the cross-sectional area of the channel.

As the working fluid flows through the channel, the frictional force arises from the interaction between the liquid/vapor and the pipe walls, which can be evaluated by

$$\frac{dp_f}{dx} = -\frac{4\tau_s}{D} \tag{2.1.6}$$

where τ_s is the frictional shear stress at the solid-liquid interface, and D is the hydraulic diameter. The shear stress may be expressed in the terms of the friction factor, f, i.e.,

$$\tau_s = \frac{1}{8} f \rho \left(\frac{dx}{dt} \right)^2 \tag{2.1.7}$$

Substituting,

$$\frac{dp_f}{dx} = -\frac{1}{2D} f \rho \left(\frac{dx}{dt} \right)^2 \tag{2.1.8}$$

Although the velocity of the working fluid in the OHP is the same for both vapor and liquid phases, the viscosity and density of the liquid phase is different from the vapor phase resulting in different pressure drops. The Reynolds numbers for liquid phase and vapor phase can be expressed as

$$\mathrm{Re}_l = \frac{\rho_l D}{\mu_l} \frac{dx}{dt} \tag{2.1.9}$$

$$\mathrm{Re}_v = \frac{\rho_v D}{\mu_v} \frac{dx}{dt} \tag{2.1.10}$$

Rearranging and solving for the density, ρ, (2.1.9) and (2.1.10) can be expressed as

$$\rho_l = \frac{\mathrm{Re}_l \, \mu_l}{D} \left(\frac{dt}{dx} \right) \tag{2.1.11}$$

$$\rho_v = \frac{\mathrm{Re}_v \, \mu_v}{D} \left(\frac{dt}{dx} \right) \tag{2.1.12}$$

(2.1.11) and (2.1.12) can then be substituted back into (2.1.8) to obtain

$$\frac{dp_f}{dx} = \frac{f \, \mathrm{Re} \, \mu L}{2 \cdot D \cdot D} \left(\frac{dt}{dx} \right) \left(\frac{dx}{dt} \right)^2 = \frac{f \, \mathrm{Re} \, \mu L}{2D^2} \frac{dx}{dt} \tag{2.1.13}$$

without reliance on the density. Utilizing the summation of the frictional pressure drops shown as

$$\Delta p_f = \Delta p_{f,l} + \Delta p_{f,v} \tag{2.1.14}$$

and substituting in for the individual phase friction pressure losses, the total frictional pressure drop can be expressed as:

$$\Delta p_f = \left[\left(f_1 \cdot \mathrm{Re}_l \right) \left(\frac{\mu_l L_l}{2D^2} \right) + \left(f_v \cdot \mathrm{Re}_v \right) \left(\frac{\mu_v L_v}{2D^2} \right) \right] \left(\frac{dx}{dt} \right) \tag{2.1.15}$$

found by integrating the frictional force equation from Eq. (2.1.8).

To obtain the final damping coefficient for the system, the total friction pressure losses is multiplied by the cross-sectional area of the channel and divided by the mean velocity, and is shown as

$$c = \frac{A \cdot \Delta p_f}{\bar{u}} = A \left[\left(f_1 \cdot \mathrm{Re}_l \right) \left(\frac{\mu_l L_l}{2D^2} \right) + \left(f_v \cdot \mathrm{Re}_v \right) \left(\frac{\mu_v L_v}{2D^2} \right) \right] \tag{2.1.16}$$

where L_v and L_l are the total lengths for the vapor bubbles and liquid plugs in the OHP, respectively. The frictional force is therefore

$$F_f = \Delta p_f A = \left[\left(f_l \cdot \mathrm{Re}_l \right) \left(\frac{\mu_l L_l}{2D^2} \right) + \left(f_v \cdot \mathrm{Re}_v \right) \left(\frac{\mu_v L_v}{2D^2} \right) \right] A \frac{dx}{dt} \tag{2.1.17}$$

To simplify future mechanical vibration calculations, the non-oscillatory term from (2.1.5) is denoted as

$$E = \left(\frac{A h_{lv} \rho_{v,c}}{T_c} \right) \left(\frac{\Delta T_{\max} - \Delta T_{\min}}{2} \right) \tag{2.1.18}$$

The law of ideal gases written in terms of mass is

$$pV = mRT \tag{2.1.19}$$

Rearranging (2.1.19) in terms of pressure of the working fluid vapor phase results in

$$p_v = \frac{m_v RT}{V_v} \tag{2.1.20}$$

If the total volume occupied by vapor at time t is V_v, i.e., $L_v A$, and vapor is assumed as an ideal gas, the vapor pressure at the time t can be found as

$$p_{v,t} = \frac{m_v RT}{L_v A} \tag{2.1.21}$$

At time $t + \Delta t$, after heat is added to the evaporating section and evaporation occurs, the increase in the pressure will result in a decrease in the vapor volume by $-xA$. If it is assumed that the vapor temperature is constant during this process, the pressure in the vapor space at time $t + \Delta t$ yields

$$p_{v,t+\Delta t} = \frac{m_v RT}{\left(L_v - x\right) A} \tag{2.1.22}$$

If x is small relative to L_v, the pressure variation at the time interval Δt can be approximately written as

$$\Delta p_v = \frac{\rho_v RT}{L_v} x \tag{2.1.23}$$

The oscillating heat pipe operates as a spring mass damper system using the compression and expansion the of working fluid vapor as a restoring force for the oscillatory motion. From the general equation for spring force,

$$F_k = \kappa x \tag{2.1.24}$$

The restoring force due to the vapor volume variation can be found as

$$F_k = A\Delta p_v = A\frac{\rho_v RT}{L_v} x \tag{2.1.25}$$

Looking at (2.1.25) in the format of (2.1.25), the spring constant can be deduced by arranging the terms to represent the isothermal process with the coefficient expressed as

$$\kappa = \frac{A\rho_v RT}{L_v} \tag{2.1.26}$$

In order to obtain the total mass of the working fluid, the definition of density is shown

$$\rho = \frac{m}{V} \tag{2.1.27}$$

which can be rewritten using the definition of volume

$$V = AL \tag{2.1.28}$$

which can be used to yield density in terms of area and length of the slugs through

$$\rho = \frac{m}{AL} \tag{2.1.29}$$

Solving (2.1.29) in terms of working fluid mass,

$$m = \rho AL \tag{2.1.30}$$

The total mass of the working fluid in both liquid and vapor phase can be written as

$$m = A\left(\rho_l L_l + \rho_v L_v\right) \tag{2.1.31}$$

According to Newton's Law, i.e., $\sum F = m\frac{d^2x}{dt^2}$, the equation governing the motion of the working fluid in an OHP can be found as

$$F_d + F_k + F_f = m\frac{d^2x}{dt^2} \tag{2.1.32}$$

Rearranging and substituting, we get

$$\begin{aligned}&\left(L_l\rho_l + L_v\rho_v\right)A\frac{d^2x}{dt^2} + \left[\left(f_l \cdot \mathrm{Re}_l\right)\left(\frac{\mu_l L_l}{2D^2}\right) + \left(f_v \cdot \mathrm{Re}_v\right)\left(\frac{\mu_v L_v}{2D^2}\right)\right]A\frac{dx}{dt} \\ &+ A\frac{\rho_v RT}{L_v}x = \left(\frac{Ah_{lv}\rho_{v,c}}{T_c}\right)\left(\frac{\Delta T_{\max} - \Delta T_{\min}}{2}\right)\left[1 + \cos\left(\omega t\right)\right]\end{aligned} \tag{2.1.33}$$

Ma et al. [14] established this model describing the motion of the working fluid in an OHP.

Examining Eq. (2.1.33), it can be found that it is a typical governing equation for forced damped mechanical vibrations, i.e.,

$$\frac{d^2x}{dt^2}+\frac{c}{m}\frac{dx}{dt}+\frac{\kappa}{m}x=\frac{E}{m}\left[1+\cos\left(\omega t\right)\right] \tag{2.1.34}$$

with substitutions from Eq. (2.1.9), Eq. (2.1.18), Eq. (2.1.26), and Eq. (2.1.31). Figure 2.2 shows a visual representation for a forced damped mechanical vibration model.

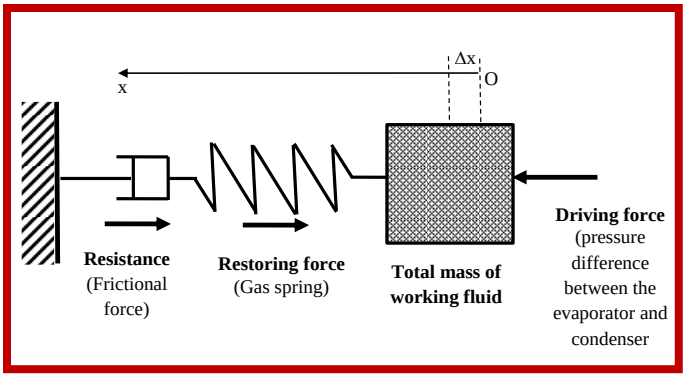

Fig. 2.2 Schematic of a forced damped mechanical vibration model

For the governing equation for forced damped mechanical vibrations, the undamped natural frequency, ω_0, and the damping ratio between actual and max damping, ζ, can be written as

$$\omega_0=\sqrt{\frac{\kappa}{m}} \tag{2.1.35}$$

and

$$\zeta=\frac{c}{2m\omega_0} \tag{2.1.36}$$

respectively.

Before heat is added on the evaporator, there is no oscillation movement in the OHP. Thus, the initial conditions for the governing equation for forced damped mechanical vibrations can be found as

$$x = 0 \quad and \quad \frac{dx}{dt} = 0; \qquad at \qquad t = 0$$

Referencing (2.1.22), the position x can be approximated using Taylor series expansion yielding

$$\Delta p_v = \frac{\rho_v RT}{L_v}\left(x + \frac{x^2}{L_v} + \frac{x^3}{L_v^2} + ... + \frac{x^n}{L_v^{n-1}} \right) \tag{2.1.37}$$

With the oscillating heat pipe operating as a forced damped mechanical vibration system, the general equation can be written as Eq. (2.1.34), but the mass can then be distributed to simplify the equation as

$$m\frac{d^2x}{dt^2} + c\frac{dx}{dt} + \kappa x = E\left(1 + \cos\left(\omega t\right)\right) \tag{2.1.38}$$

Substituting in the new x value from (2.1.37), (2.1.33) can be rewritten as

$$\begin{aligned} &\left(L_l\rho_l + L_v\rho_v\right)A\frac{d^2x}{dt^2} + \left[\left(f_l \cdot \mathrm{Re}_l\right)\left(\frac{\mu_l L_l}{2D^2}\right) + \left(f_v \cdot \mathrm{Re}_v\right)\left(\frac{\mu_v L_v}{2D^2}\right)\right]A\frac{dx}{dt} \\ &+ A\frac{\rho_v RT}{L_v}\left(x + \frac{x^2}{L_v} + \frac{x^3}{L_v^2} + ... + \frac{x^n}{L_v^{n-1}} \right) = \left(\frac{Ah_{lv}\rho_{v,c}}{T_c}\right)\left(\frac{\Delta T_{\max} - \Delta T_{\min}}{2}\right)\left[1 + \cos\left(\omega t\right)\right] \end{aligned} \tag{2.1.39}$$

The governing equation for forced damped mechanical vibrations is simply a nonhomogeneous, second-order ordinary differential equation (ODE) where the exact solution is subject to the boundary conditions given above. Utilizing Laplace transforms, the exact solution can be readily obtained, i.e.,

$$x(t) = \frac{E}{m}\left[\begin{array}{l} \dfrac{\left(\sqrt{\zeta^2 - 1}\right)\sin\left(\omega t\right) - e^{-\zeta\omega t}\sinh\left[\omega\left(\sqrt{\zeta^2 - 1}\right)t\right]}{2\zeta\omega^2\sqrt{\zeta^2 - 1}} \\ + \dfrac{1 - e^{-\zeta\omega t}\left[\cosh\left(\left(\sqrt{\zeta^2 - 1}\right)\omega t\right) + \dfrac{\zeta\sinh\left(\left(\sqrt{\zeta^2 - 1}\right)\omega t\right)}{\sqrt{\zeta^2 - 1}}\right]}{\omega^2} \end{array}\right] \tag{2.1.40}$$

Eq. (2.1.40) can then be used to create theoretical models of the oscillatory movement of the working fluid with given OHP parameters. These models can then be used to find the amplitude and frequency of the working fluid with given parameters in order to determine the average velocity of the working fluid inside the OHP at steady-state.

2.1.2 Heat Transfer in the Evaporating Section of an Oscillating Heat Pipe

When heat is applied to the external section of the evaporator as shown in Fig. 2.3, it is first transferred via conduction through the walls until it reaches the working fluid at which point the fluid starts vaporizing. This vaporization leads to a vapor volume expansion in the evaporator section and a corresponding vapor volume contraction reaction in the condenser section as liquid condenses. This expansion and contraction of the vapor volume causes the oscillating motion leading to forced convection. If the tube structuring the evaporating section is smooth, i.e., no wick structures on the inside surface of tube, the heat transfer process occurring in the evaporating section is similar to convection boiling heat transfer, which has been extensively investigated [18–25].

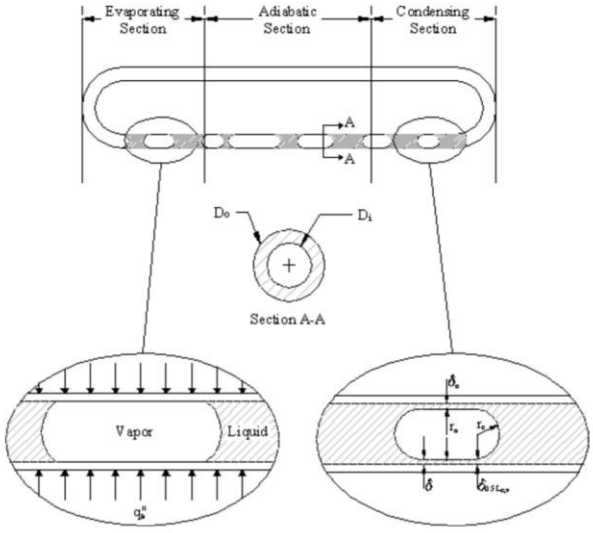

Fig. 2.3 Schematic of the vapor bubbles and liquid plugs inside an OHP

The heat transfer in the evaporating section is a combination of nucleate boiling and bulk convection. Between these two forms of convective heat transfer, the total heat transfer coefficient h is expressed as

$$h_{total,e} = h_{mic} + h_{mac} \tag{2.1.41}$$

where h_{mic} is due to the nucleate boiling heat transfer and h_{mac} is due to the bulk convection that results from the oscillating motions. The microscopic nucleate boiling portion of the heat transfer coefficient can be derived from the Nusselt number found by Forster and Zuber [18] for the case of pool boiling such that

$$Nu_d = 0.0015\left(\mathrm{Re}_b\right)^{0.62}\left(\mathrm{Pr}_l\right)^{0.33} = \frac{h_b r_b}{k_l} \tag{2.1.42}$$

where r_b is the bubble radius and Re_b is the Reynolds number for micro-convective boiling heat transfer, and are defined, respectively, as

$$r_b = \frac{\Delta T}{h_{lv}\rho_v}\left(\frac{2\pi k_l c_{p,l}\sigma}{\Delta p}\right)^{0.5}\left(\frac{\rho_l}{g_c \Delta p}\right)^{0.25} \tag{2.1.43}$$

$$\mathrm{Re}_b = \left(\frac{\pi k_l c_{p,l}}{\mu_l}\right)\left(\frac{\rho_l \Delta T}{\rho_v h_{lv}}\right)^2 \tag{2.1.44}$$

These equations are based on the premise that the Reynolds number for micro-convective boiling heat transfer is governed by the growth rate of bubbles. This rate is described by the Rayleigh equation which Forster and Zuber solved to show that the product of the bubble radius and the bubble growth rate is a constant for a specific superheat. For the case of boiling from a superheated wall, whether in pool boiling or convective boiling, the degree of superheat actually is not constant across the boundary layer. Due to this fact, the Reynolds number used in the Forster-Zuber equation actually is an effective Reynolds number representative of some mean,

effective super-heat. The difference between this effective superheat and the wall super-heat is small for the case of pool boiling and was neglected in Forster and Zuber's derivation. However, this difference cannot be neglected in the case of convective boiling since the temperature gradient is now dependent on flow rate and vapor quality and would generally be much steeper than in the corresponding pool boiling case with the same wall super-heat.

In using Forster and Zuber's formulation to represent micro-convective heat transfer in convective boiling, this effect was taken into account by writing Eq. (2.1.42), Eq. (2.1.43), and Eq. (2.1.44) in terms of effective ΔT and ΔP, which in this case, is Eq. (2.1.45).

$$h_{mic} = 0.00122\left[\frac{k_l^{0.79} c_{pl}^{0.45} \rho_l^{0.49}}{\sigma^{0.5} \mu_l^{0.29} h_{lv}^{0.24} \rho_v^{0.24}}\right]\left[T_w - T_{sat}\left(P_l\right)\right]^{0.24}\left[P_{sat}\left(T_w\right) - P_l\right]^{0.75} S \tag{2.1.45}$$

This model was developed by Chen [18] which describes the microscopic nucleate boiling portion of the heat transfer coefficient. S is a suppression factor and a function of the two-phase Reynolds number, which is

$$S = \left(1 + 2.56\times10^{-6}\,\mathrm{Re}_{tp}^{1.17}\right)^{-1} \tag{2.1.46}$$

where the two-phase Reynolds number is defined as

$$\mathrm{Re}_{tp} = \mathrm{Re}_l\left[F\left(X_{tt}\right)\right]^{1.25} \tag{2.1.47}$$

and where Re_l is the liquid Reynolds and X_{tt} is the Martinelli parameter. The liquid Reynolds number is found by first defining the mass flux G such that

$$G = \frac{\dot{m}}{A} = \frac{uA\rho_l}{A} = u\rho_l \tag{2.1.48}$$

and where the general equation for the Reynolds number is

$$\mathrm{Re} = \frac{u\rho D_i}{\mu} \tag{2.1.49}$$

When considering only the liquid portion of the fluid, Eq. (2.1.49) is multiplied by the liquid percentage of the total working fluid in terms of the vapor quality such that

$$\mathrm{Re}_l = \frac{G(1-x)D_i}{\mu_l} \tag{2.1.50}$$

The Martinelli parameter is derived such that

$$\left(\frac{\Delta p_f}{L}\right)_{tp} = \phi_l^2 \left(\frac{\Delta p_f}{L}\right) \tag{2.1.51}$$

where ϕ_l^2 is the two-phase frictional multiplier for liquid flow and is defined as

$$\phi_l^2 = 1 + \frac{c}{x} + \frac{1}{x^2} \tag{2.1.52}$$

and the generic Martinelli parameter is given as

$$X_{tt} = \left[\frac{\left(\frac{\Delta p_f}{L}\right)_l}{\left(\frac{\Delta p_f}{L}\right)_v}\right]^{0.5} \tag{2.1.53}$$

For the case where both the gaseous and liquid flow are both turbulent, the two-phase frictional factor for the liquid is shown to be

$$\phi_l^2 = 1 + \frac{c}{X_{tt}} + \frac{1}{X_{tt}^2} \tag{2.1.54}$$

The Fanning friction factor is defined as

$$f = \frac{const.}{\mathrm{Re}^n} \tag{2.1.55}$$

A proportionality relationship may then be found such that

$$\frac{\Delta p_f}{L} \propto \frac{fG^2}{s} \propto G^{2-n}\mu^n s^{-1} \propto \dot{m}^{2-n}\mu^n s^{-1} \tag{2.1.56}$$

where it follows that

$$\left(\frac{\Delta p_f}{L}\right)^{0.5} \propto \dot{m}^{\frac{(2-n)}{2}} \mu^{n/2} s^{-0.5} \tag{2.1.57}$$

A relationship for the generic Martinelli parameter may then be expressed as

$$X_{tt} = \left(\frac{\dot{m}_l}{\dot{m}_v}\right)^{\frac{(2-n)}{2}} \left(\frac{\mu_l}{\mu_v}\right)^{\frac{n}{2}} \left(\frac{s_v}{s_l}\right)^{0.5} \tag{2.1.58}$$

where $\dot{m}_l = \dot{m}(1-x)$ and $\dot{m}_v = \dot{m}x$. Substituting these into Eq. (2.1.58) gives

$$X_{tt} = \left(\frac{1-x}{x}\right)^{\frac{(2-n)}{2}} \left(\frac{\rho_v}{\rho_l}\right)^{0.5} \left(\frac{\mu_l}{\mu_v}\right)^{\frac{n}{2}} \tag{2.1.59}$$

For the case where both the gaseous and liquid flow are turbulent, $n = 0.2$ which gives

$$X_{tt} = \left(\frac{1-x}{x}\right)^{0.9} \left(\frac{\rho_v}{\rho_l}\right)^{0.5} \left(\frac{\mu_l}{\mu_v}\right)^{0.1} \tag{2.1.60}$$

The function $F(X_{tt})$ in Eq. (2.1.47) depends on the Martinelli parameter and is defined as

$$F\left(X_{tt}\right) = 1 \quad \text{for} \quad X_{tt}^{-1} > 0.1 \tag{2.1.61}$$

$$F\left(X_{tt}\right) = 2.35\left(0.213 + \frac{1}{X_{tt}}\right)^{0.736} \quad \text{for} \quad X_{tt}^{-1} > 0.1 \tag{2.1.62}$$

When the filling ration ϕ is known, the quality is derived such that

$$x = \frac{m_v}{m_t} = \frac{\rho_v V_v}{\overline{\rho} V_t} = \frac{\rho_v}{\overline{\rho}}\left(1-\phi\right) = \frac{\rho_v - \phi\rho_v}{\overline{\rho}} \tag{2.1.63}$$

where the average density of working fluid in the system may be calculated from the definition of specific volume as

$$v = xv_v + (1-x)v_l \tag{2.1.64}$$

where $v = 1/\rho$ which results in

$$\frac{1}{\rho} = \frac{x}{\rho_v} + \frac{1-x}{\rho_l} \tag{2.1.65}$$

Utilizing the Martinelli parameter for a two-phase flow, the heat transfer coefficient due to the forced convection caused by oscillating motions (macroscopic heat transfer coefficient) can be readily determined by

$$h_{mac} = F\left(X_{tt}\right) h_l \tag{2.1.66}$$

where $F\left(X_{tt}\right)$ is the Martinelli function seen in Eq (2.1.61) and Eq. (2.1.62). The Martinelli function adjusts for a two-phase flow scenario, where

$$\begin{aligned} X_{tt} &\ll 1 \qquad \textit{Gas Flow} \\ X_{tt} &\approx 1 \qquad \textit{Two-Phase Flow} \\ X_{tt} &\gg 1 \qquad \textit{Liquid Flow} \end{aligned}$$

Knowing $Nu_D = \frac{h_l D}{k_l}$ and rearranging to get $h_l = \frac{k_l Nu_D}{D}$, the Dittus-Boelter equation states

$$Nu_D = 0.023 \mathrm{Re}_D^{0.8} \mathrm{Pr}_l^n \tag{2.1.67}$$

Where

$$\begin{aligned} n &= 0.4 \qquad \textit{for heating} \\ n &= 0.33 \qquad \textit{for cooling} \end{aligned} \tag{2.1.68}$$

The Dittus-Boelter equation is a good approximation for a fully developed turbulent flow in a smooth circular tube where temperature differences between bulk fluid and heat transfer surface are minimal, avoiding equation complexity and iterative solving. Therefore,

$$h_l = 0.023\left(\frac{k_l}{D}\right)\mathrm{Re}_l^{0.8} \mathrm{Pr}_l^{0.4} \tag{2.1.69}$$

The temperature difference in the evaporator section is therefore

$$\Delta T_e = \frac{q_e^{"}}{h_{total,e}} \tag{2.1.70}$$

where L_e is the length of the evaporator section.

2.1.3 Heat Transfer in the Condensing Section of an Oscillating Heat Pipe

The vapor generated in the evaporating section is condensed in the condensing section if the phase-change driving force exists, and the condensate in the thin film region will flow into the liquid-slug region due to the capillary force. Because the film thickness in the condensing film region is very thin compared to the meniscus thickness in the liquid slug, most of the condensing heat transfer will occur in the thin film region. In this region, the Reynolds number of the condensate is very small; hence the inertial terms can be neglected and based on conservation of momentum in the thin film, the pressure drop due to the viscous flow can be found as

$$\frac{dP_l}{ds} = \frac{f\,\mathrm{Re}_\delta\,\mu_l D_o q_c^{"} s}{2\delta^3 D_i \rho_l h_{fg}} \tag{2.1.71}$$

where s is the coordinate along the condensing film starting from the middle point of the condensing film and δ is the thin film thickness. Knowing that the general equation for the Reynold's number of a fluid is

$$\mathrm{Re} = \frac{\rho u L}{\mu} \tag{2.1.72}$$

the Reynold's number of the condensing film can be found as

$$\mathrm{Re}_\delta = \frac{\overline{U_{l,c}}\delta\rho_l}{\mu_l} \tag{2.1.73}$$

where $\overline{U_{l,c}}$ is the average velocity of the condensate.

By integrating the equation for pressure drop due to the viscous flow from $s = 0$ to $\frac{L_{c,v}}{2}$, the total pressure drop along half of the vapor bubble length can be found as

$$\Delta P_l = \int_0^{\frac{L_{c,v}}{2}} \left(\frac{f \cdot \mathrm{Re}_\delta \, \mu_l D_0 q_c^{"}}{2\delta^3 D_i \rho_l h_{lv}} \right) sds \tag{2.1.74}$$

There exist numerous vapor slugs in the OHP including the condensing section. Although the vapor slug distributions, i.e., vapor bubble number, in the OHP is unpredictable, the total vapor space remains constant for a given liquid filling ratio ϕ, which is defined as

$$\phi = \frac{V_l}{V_{total}} \tag{2.1.75}$$

where V_l is the volume occupied by liquid, and V_{total} is the total volume throughout the oscillating heat pipe.

In the condenser, it is assumed that all the vapor bubbles are combined with the condensing taking place on the perimeter of the large slug. When a uniform distribution of vapor throughout the length of the heat pipe is assumed, the length of the idealized single vapor slug in the condenser may be found such that

$$L_{c,v} = L_c \left(1 - \phi\right) \tag{2.1.76}$$

Knowing that the Laplace Young Eq is

$$P_I - P_{II} = \sigma \left(\frac{1}{r_1} + \frac{1}{r_2} \right) \tag{2.1.77}$$

and making the assumption that $r_1 = r_2$, we get

$$P_I - P_{II} = \frac{2\sigma}{r} \text{ at liquid-vapor interface} \tag{2.1.78}$$

It is known that K is the curvature and is defined as

$$K = \frac{\frac{d^2\delta}{dx^2}}{\left[1+\left(\frac{d\delta}{dx}\right)^2\right]^{3/2}} \tag{2.1.79}$$

which is

$$K = \frac{1}{r_t} \tag{2.1.80}$$

for a capillary tube. Substituting, the resulting equation for capillary pressure results in

$$\Delta P_C = 2\sigma K \tag{2.1.81}$$

After deriving along the condensate film, the derived equation is

$$\frac{dP_c}{ds} = 2\sigma \frac{dK}{ds} \tag{2.1.82}$$

Rearranging Eq. (2.1.82), we get $dP_c = 2\sigma dK$ and then Integrating from $K = \frac{1}{r_0}$ to $K = \frac{1}{r_c}$, the total capillary pressure can be found as

$$\Delta P_c = 2\sigma \int_{\frac{1}{r_0}}^{\frac{1}{r_c}} dK \tag{2.1.83}$$

which simplifies to

$$\Delta P_c = \sigma\left(\frac{2}{r_c} - \frac{1}{r_0}\right) \tag{2.1.84}$$

where r_0 is the meniscus radius of the liquid-vapor interface at the line of symmetry, s = 0 and r_c is the meniscus radius of the liquid-vapor interface at the liquid slug, s = $L_{c,v}$ which can be found from Fig. 2.3, respectively, as

$$r_0 = \frac{1}{2}\left(D_i - 2\delta_0\right) \tag{2.1.85}$$

and

$$r_c = \frac{1}{2}\left(D_i - 2\delta_{0.5L_{c,v}}\right) \tag{2.1.86}$$

When considering Eq. (2.1.85) and Eq. (2.1.86), the total capillary pressure can be rewritten as

$$\Delta P_c = \sigma\left(\frac{2}{\left(\frac{D_i}{2} - \delta_{0.5L_{c,v}}\right)} - \frac{1}{\left(\frac{D_i}{2} - \delta_0\right)}\right) \tag{2.1.87}$$

For the steady-state condensation process of the thin film, the capillary pressure defined in Eq. (2.1.87) should be equal to the pressure drop determined by Eq. (2.1.74). Setting the equations equal to each other and rearranging, the film thickness can be found as

$$\delta = \sqrt[3]{\frac{\left(\frac{f\,\mathrm{Re}_\delta\,\mu_l D_o q_c'' L_{c,v}^2}{16 D_i \rho_l h_{fg}}\right)}{\sigma\left(\frac{2}{\left(\frac{D_i}{2} - \delta_{0.5L_{c,v}}\right)} - \frac{1}{\left(\frac{D_i}{2} - \delta_0\right)}\right)}} \tag{2.1.88}$$

With a given heat flux, Eq. (2.1.88) may be solved, and the condensation film thickness determined. The temperature difference in the condensing section can then be found using

$$\Delta T_c = \frac{q_c''\delta}{k_l} \tag{2.1.90}$$

2.2 Hybrid Fluid Selection for the Hybrid Fluid Oscillating Heat Pipe

When an OHP is filled with a hybrid fluid and heat is applied in the evaporator, the water evaporates into saturated vapor, whereas the liquid metal remains a liquid (depending on what materials are being used). This leads to a train of liquid metal plugs and vapor bubbles as shown in Fig. 2.4.

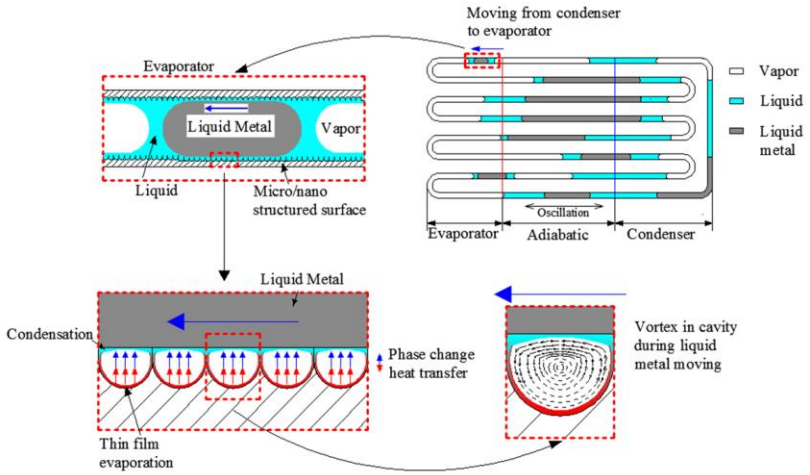

Fig. 2.4 Schematic of hybrid fluid interaction in a HFOHP

Analyzing closely, there is thin film evaporation and condensation occurring in the HFOHP, as shown in Fig. 2.5.

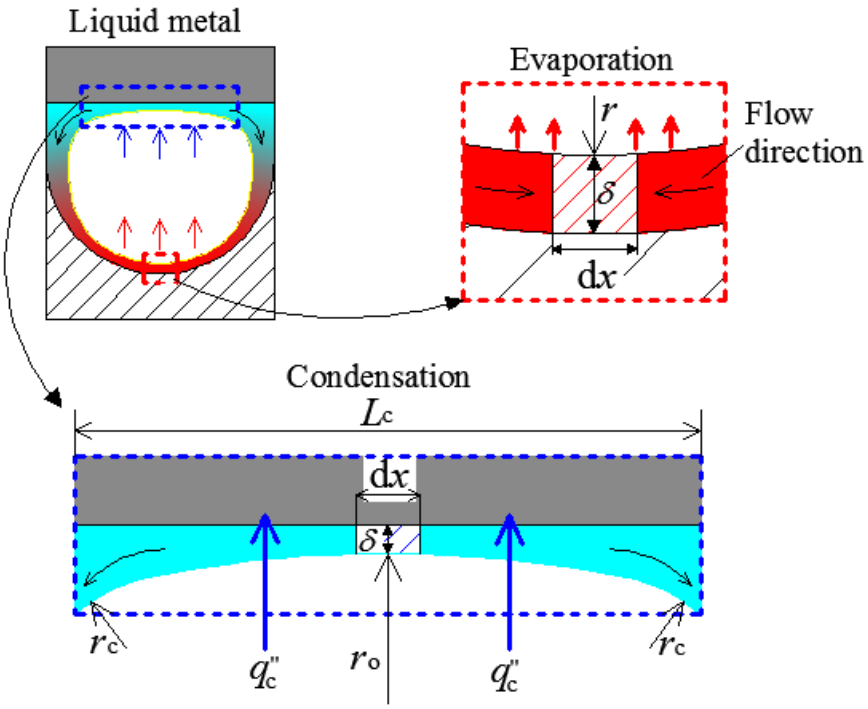

Fig. 2.5 Schematic of thin film evaporation and condensation in a HFOHP

With these effects in mind, a hybrid fluid of gallium and water is used for this investigation. The reason is due to gallium and its alloys being the best candidates for heat transfer management under 100 °C working temperatures, due to their low melting point. Furthermore, the surface tension of gallium is nearly 10 times higher than that of water [17], implying that galinstan can hold a ball shape on a surface and be in a nonwetting state. The wetting condition of gallium and water on a rough surface is shown in Fig. 2.6.

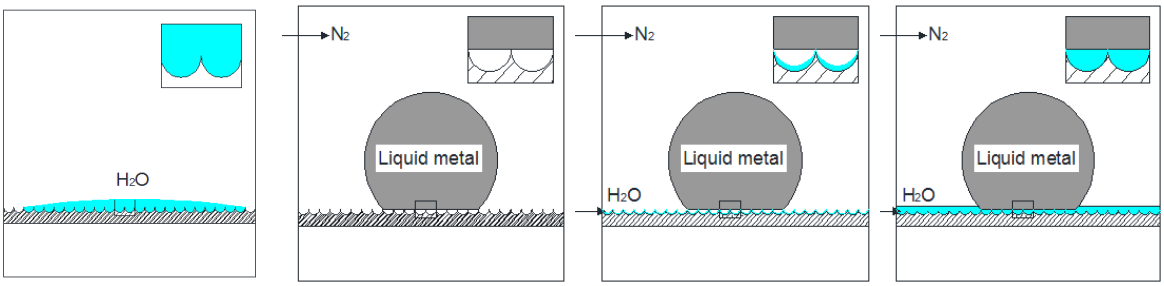

Fig. 2.6 Wetting condition on the rough surface of a HFOHP

Figures 2.7-2.10 show the previous visual observations made on a HFOHP based on research by Hao et al. [26]. It was observed that liquid metal tends to stay towards the bottom of the OHP, and that the liquid metal column become small balls.

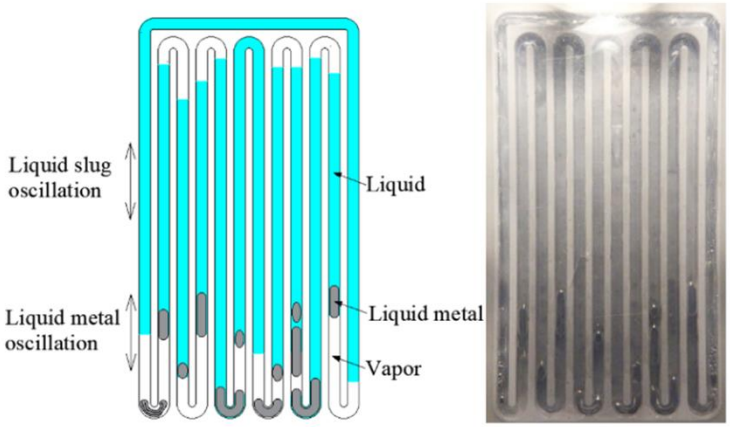

Fig. 2.7 First visual observation made of a HFOHP

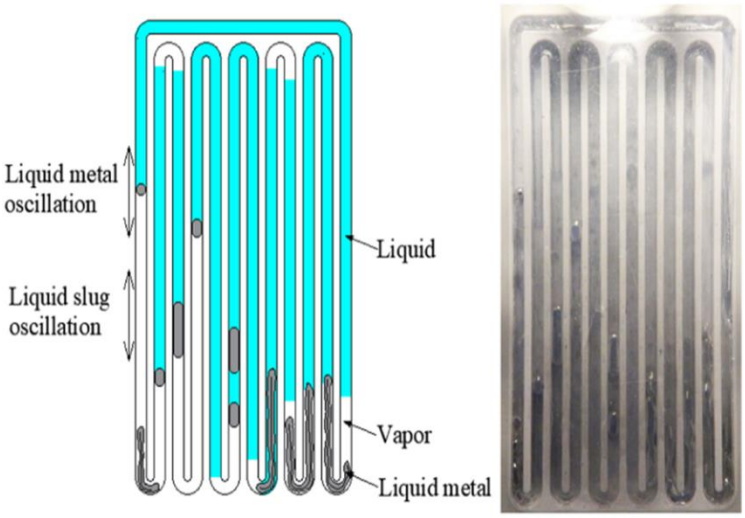

Fig. 2.8 Second visual observation made of a HFOHP

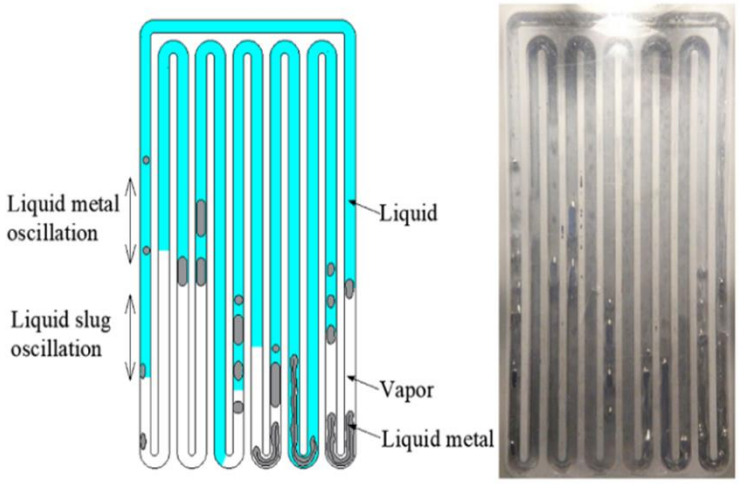

Fig. 2.9 Third visual observation made of a HFOHP

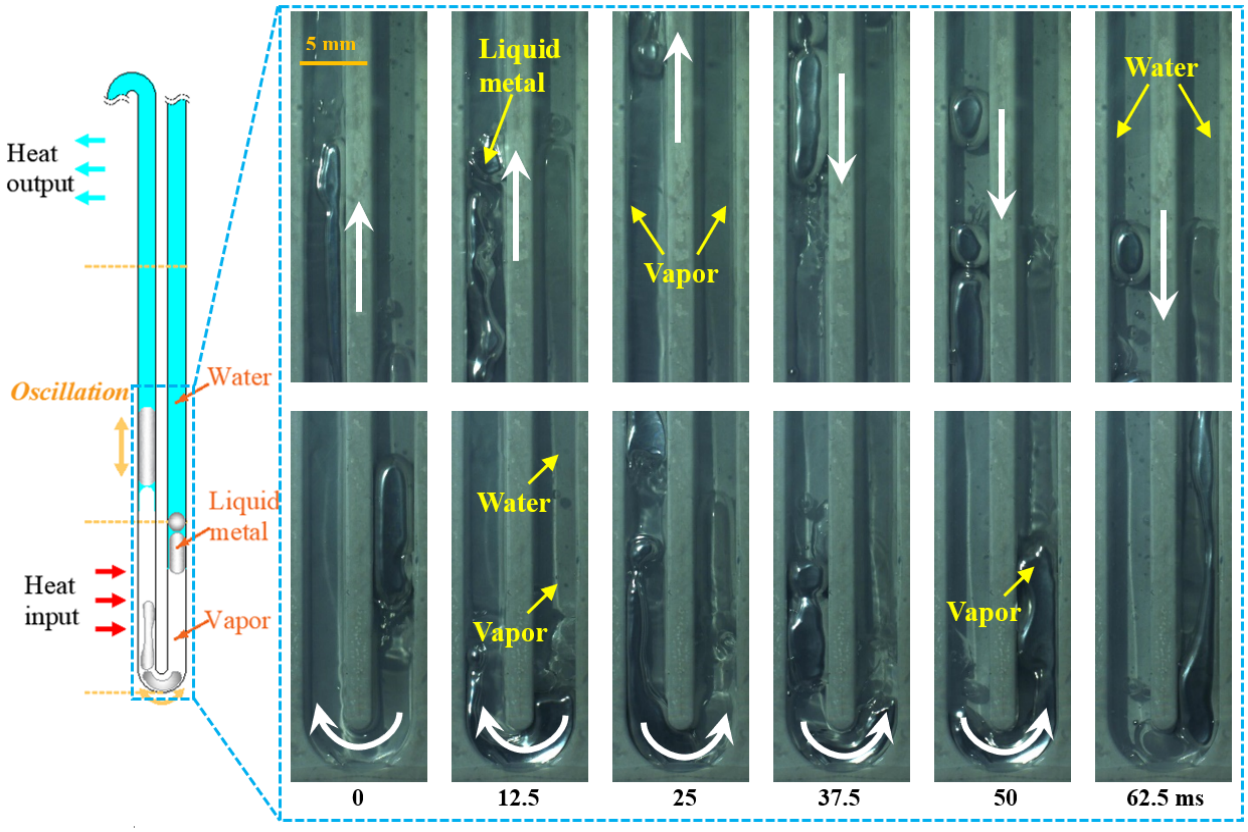

Fig. 2.10 Closer visual observation of a HFOHP

For the galinstan–silicon dioxide–nitrogen system, the advancing contact angle under nonoxidizing conditions has been experimentally determined to be 146.8°. Gallium flow resistance is reduced on the micro/nanostructured surface. Recently, Lam et al. [27] analytically investigated the hydrodynamic slip of galinstan on the microstructured surface, and the microstructured surfaces effect on the overall thermal resistance of a galinstan-based microgap cooling in the laminar flow regime. The overall thermal resistance was reduced during the galinstan-based microgap cooling. Many previous works [28-30] have modeled the hydrodynamic slip on superhydrophobic surface. A review of experimental and theoretical hydrodynamic work was conducted by Rothstein [31]. The flow resistance reduction and higher thermal conductivity of liquid metal will significantly help to increase the heat transfer

performance of a standard OHP. The properties of the hybrid fluid chosen are shown in Table 2.1.

Table 2.1 Properties of the hybrid fluid chosen (gallium + water)

	Gallium	Water
Melting point [°C]	29.76	0
Boiling point [°C]	2,400	100
Vapor pressure [mmHg]	$<10^{-8}$ at 500°C	760 at 100°C
Specific heat [kJ/(kg*°C)]	0.37 at 30°C	4.183 at 20°C
Density [kg/m^3]	5900 at 30°C	998.2 at 20°C
Thermal conductivity [W/(m*°C)]	24 at 30°C	0.599 at 20°C
Solubility in water	Insoluble	-
Dynamic viscosity [Pa*s]	$2.4\text{x}10^{-3}$ at 30°C	$1.005\text{x}10^{-3}$ at 20°C
Surface tension [N/m]	0.725 at 30°C	0.0727 at 20°C

In order to be able to calculate and simulate the mathematical models, the hybrid fluid has to be treated as a theoretical mixture in order to have single values pertaining to the hybrid fluid's thermal properties. The first thermal property treated as a theoretical mixture is the liquid density of the hybrid fluid, which is calculated using the relation

$$\rho_{HF} = \frac{\left(m_1 + m_2\right)}{\left(V_1 + V_2\right)} \tag{2.1.91}$$

The second thermal property treated as a theoretical mixture is the liquid specific heat of the hybrid fluid, which is calculated using the relation

$$c_{p,HF} = \left(\frac{m_1}{m_{total}}\right) c_{p,1} + \left(\frac{m_2}{m_{total}}\right) c_{p,2} \tag{2.1.92}$$

The third thermal property treated as a theoretical mixture is the liquid dynamic viscosity of the hybrid fluid, which is calculated using the Kendall-Monroe equation [32], which is

$$\mu_{HF} = \left(Y_1\mu_1^{1/3} + Y_2\mu_2^{1/3}\right)^3 \tag{2.1.93}$$

where Y is the mole fraction. The fourth thermal property treated as a theoretical mixture is the liquid thermal conductivity of the hybrid fluid, which is calculated using the Jamieson and Irving equation [33], which is

$$k_{l,HF} = k_{l,1}y_1 + k_{l,2}y_2 - \left(k_{l,1} - k_{l,2}\right)\left(1 - \sqrt{y_1}\right)y_1, \qquad k_1 > k_2 \tag{2.1.94}$$

where y is the mass fraction. The fifth thermal property treated as a theoretical mixture is the liquid surface tension of the hybrid fluid, which is calculated using the ideal surface tension equation, which is

$$\sigma_{HF} = Y_1\sigma_1 + Y_2\sigma_2 \tag{2.1.94}$$

After these values are calculated, simulation of the mathematical models can now be performed.

2.3 Simulation

2.3.1 Setup

The theoretical simulation of the oscillatory motion as well as the heat transfer of a HFOHP was conducted through MATLAB. MATLAB is a proprietary multi-paradigm programming language and numeric computing environment developed by MathWorks. MATLAB allows matrix manipulations, plotting of functions and data, implementation of algorithms, creation of user interfaces, and interfacing with programs written in other languages. The MATLAB simulation was coded from scratch using the mathematical model derived earlier.

2.3.2 Results and Discussion

Using the equations shown and creating an analytical code in MATLAB for a HFOHP under different conditions, analytical models are obtained. Figures 2.11-2.20 show analytical models of theoretical oscillating motions for both water as well as a hybrid fluid (15% gallium and 85% water) in an OHP at different operating conditions, where all filling ratio percentages are in regard to volumetric percentages.

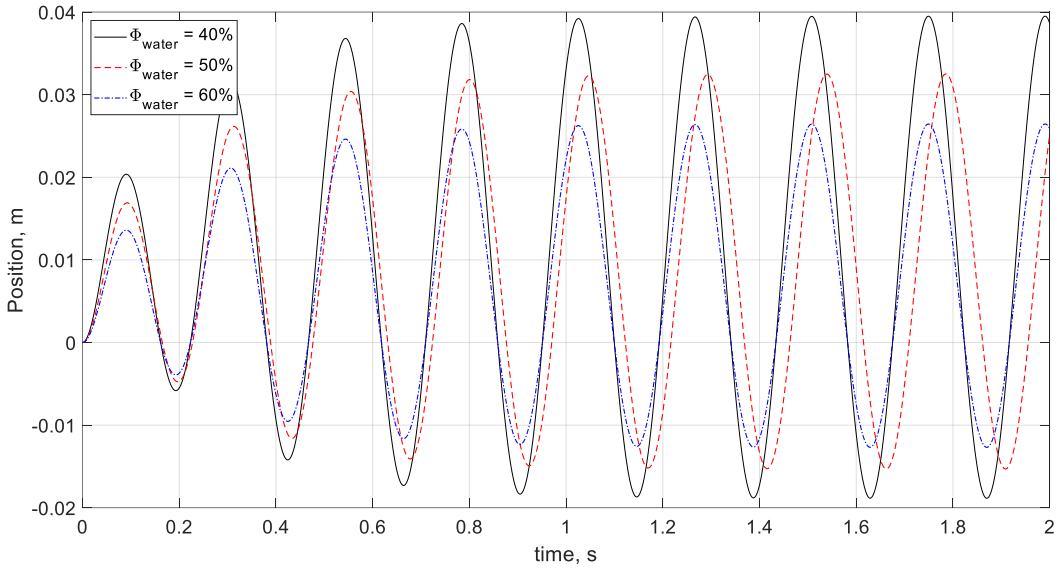

Fig. 2.11 Analytical model showing theoretical oscillating motion for water in an OHP at different filling ratios with characteristic length of 107 mm, inner diameter of 2 mm, operating temperature of 15 °C, and maximum temperature difference of 5 °C

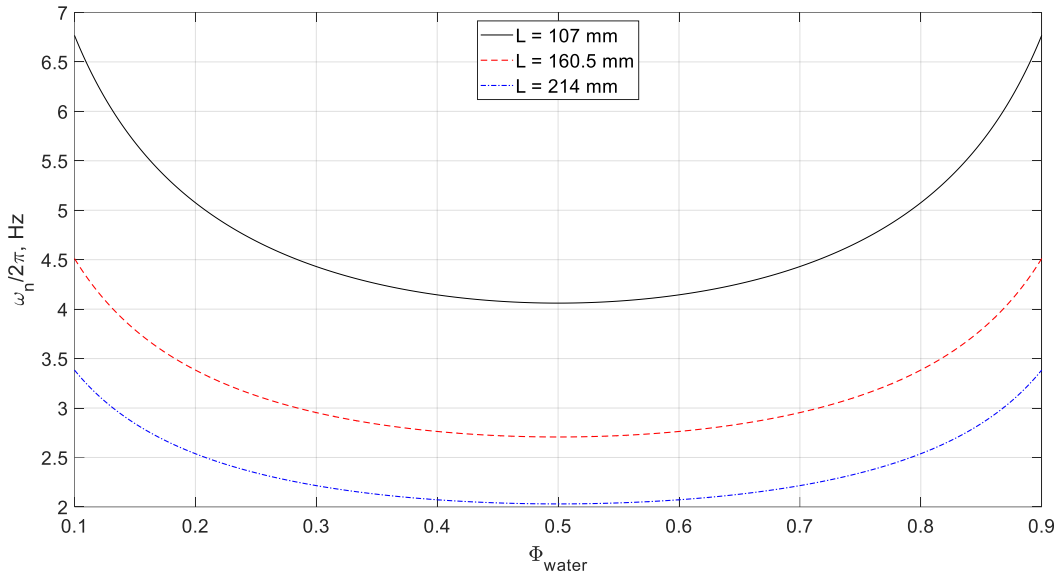

Fig. 2.12 Analytical model showing theoretical oscillating frequency for water in an OHP at different filling ratios and characteristic lengths with inner diameter of 2 mm, operating temperature of 15 °C, and temperature difference of 5 °C

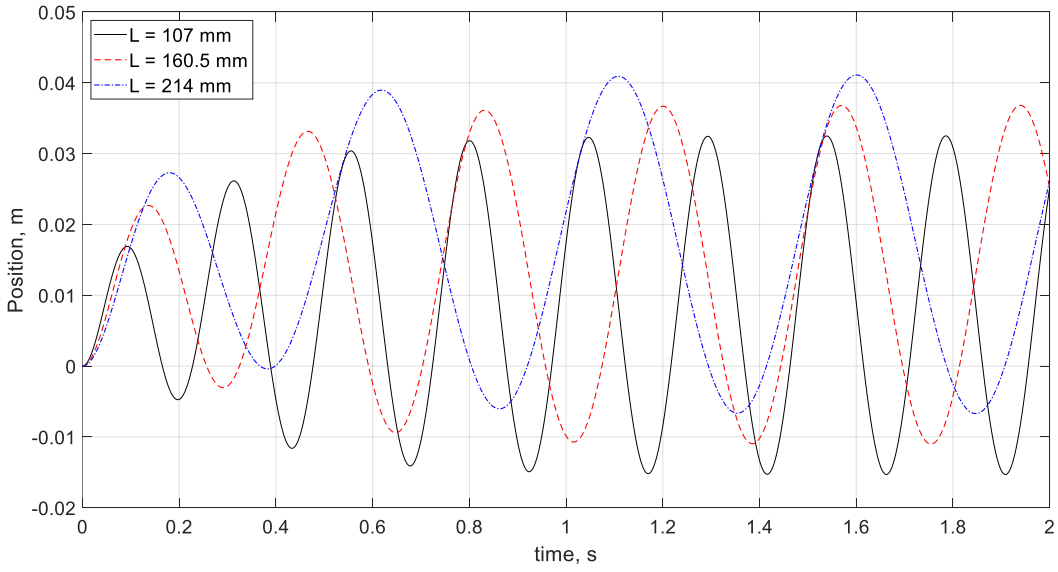

Fig. 2.13 Analytical model showing theoretical oscillating motion for water in an OHP at different characteristic lengths with filling ratio of 50%, diameter of 2 mm, operating temperature of 15 °C, and temperature difference of 5 °C

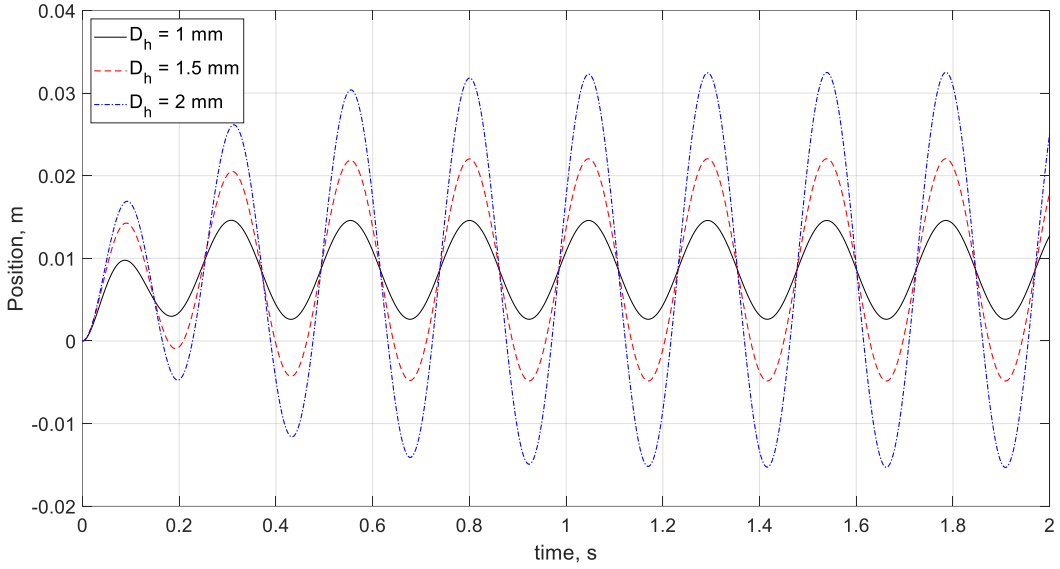

Fig. 2.14 Analytical model showing theoretical oscillating motion for water in an OHP at different inner hydraulic diameters with filling ratio of 50%, characteristic length of 107 mm, operating temperature of 15 °C, and temperature difference of 5 °C

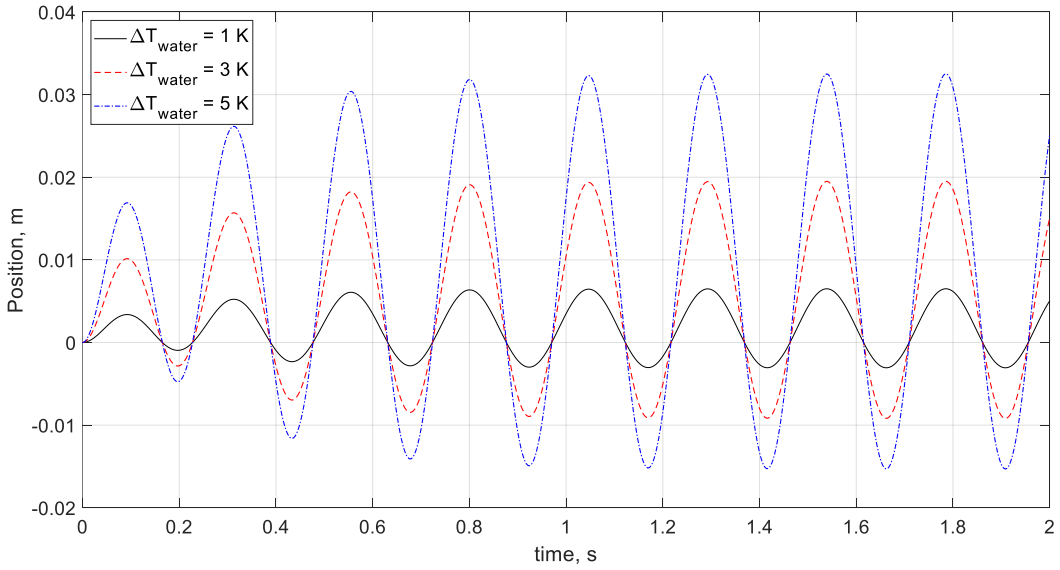

Fig. 2.15 Analytical model showing theoretical oscillating motion for water in an OHP at different temperature differences with filling ratio of 50%, characteristic length of 107 mm, inner diameter of 2 mm, and operating temperature of 15 °C

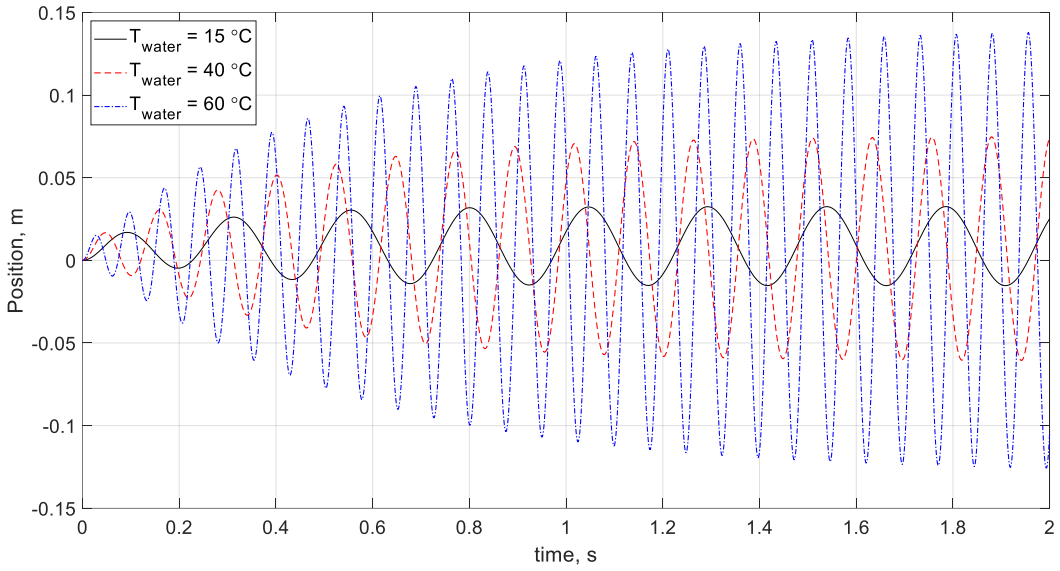

Fig. 2.16 Analytical model showing theoretical oscillating motion for water in an OHP at different operating temperatures with characteristic length of 107 mm, inner diameter of 2 mm, filling ratio of 50%, and temperature difference of 5 °C

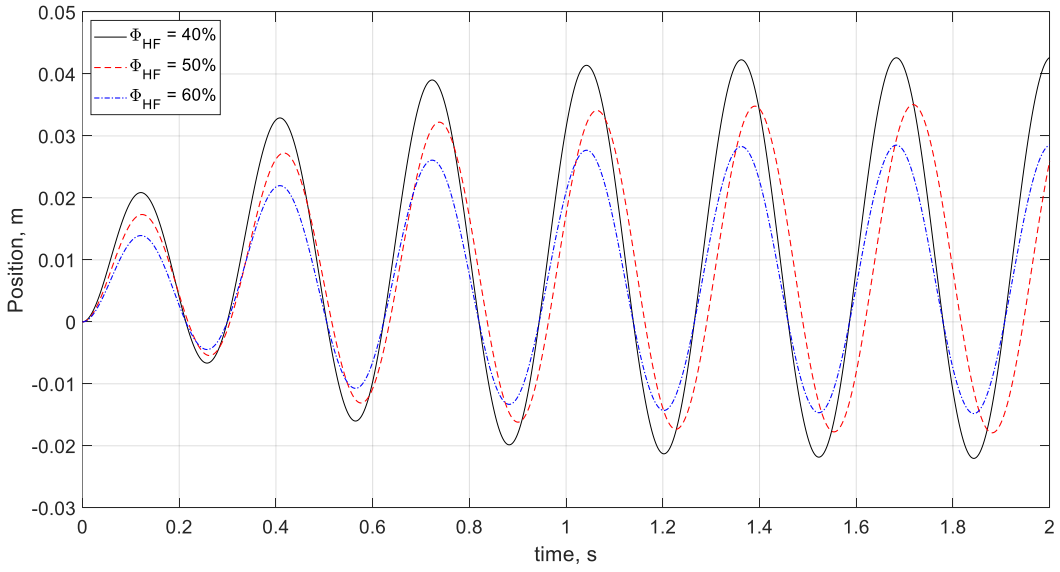

Fig. 2.17 Analytical model showing theoretical oscillating motion for a hybrid fluid of 15% gallium and 85% water in an OHP at different filling ratios with characteristic length of 107 mm, diameter of 2 mm, operating temperature of 15 °C, and temperature difference of 5 °C

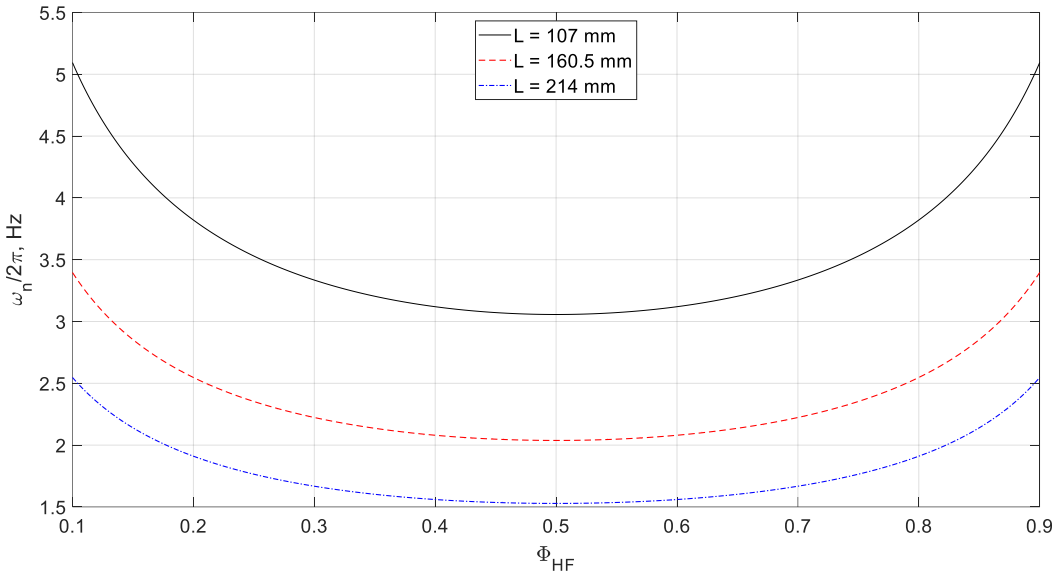

Fig. 2.18 Analytical model showing theoretical oscillating frequency for a hybrid fluid of 15% gallium and 85% water in an OHP at different filling ratios and characteristic lengths with inner diameter of 2 mm, operating temperature of 15 °C, and temperature difference of 5 °C

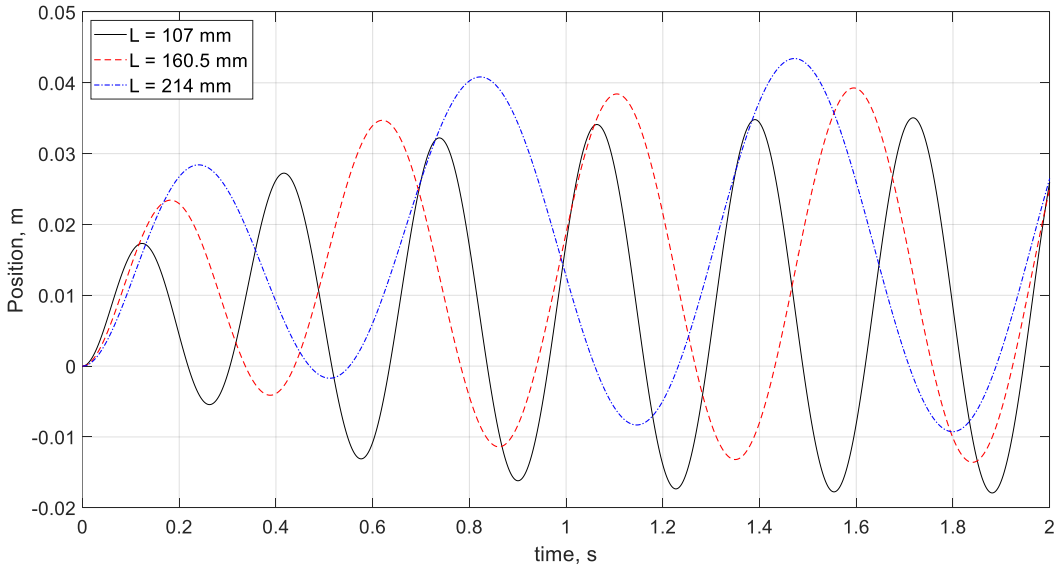

Fig. 2.19 Analytical model showing theoretical oscillating motion for a hybrid fluid of 15% gallium and 85% water in an OHP at different characteristic lengths with filling ratio of 50%, inner diameter of 2 mm, operating temperature of 15 °C, and temperature difference of 5 °C

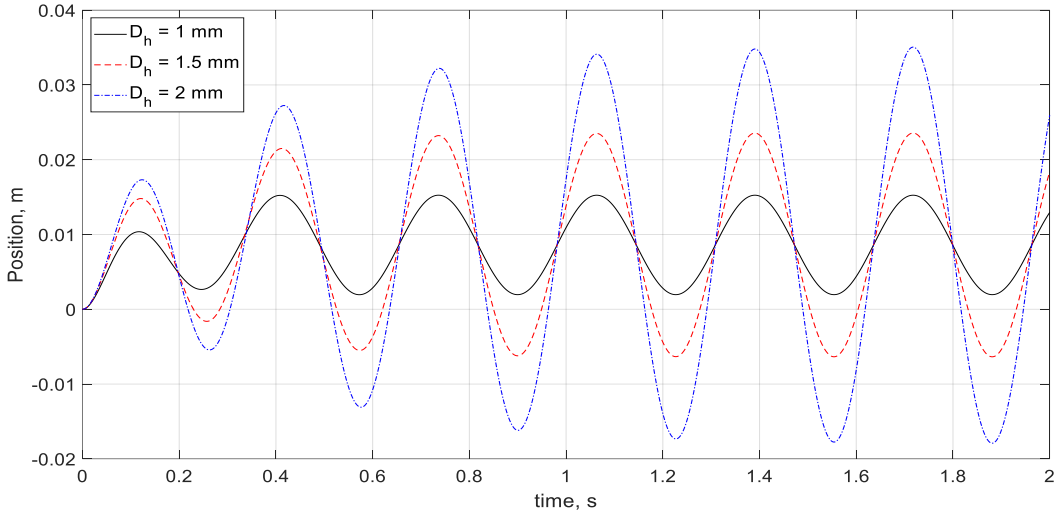

Fig. 2.20 Analytical model showing theoretical oscillating motion for a hybrid fluid of 15% gallium and 85% water in an OHP at different inner hydraulic diameters with filling ratio of 50%, characteristic length of 107 mm, operating temperature of 15 °C, and temperature difference of 5 °C

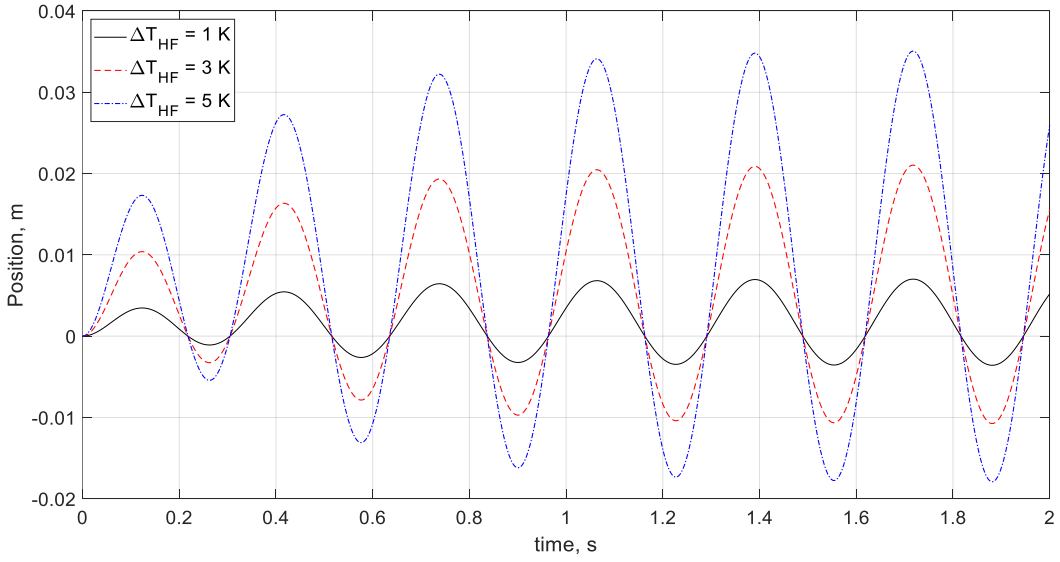

Fig. 2.21 Analytical model showing theoretical oscillating motion for a hybrid fluid of 15% gallium and 85% water in an OHP at different temperature differences with filling ratio of 50%, characteristic length of 107 mm, operating temperature of 15 °C, and inner diameter of 2 mm

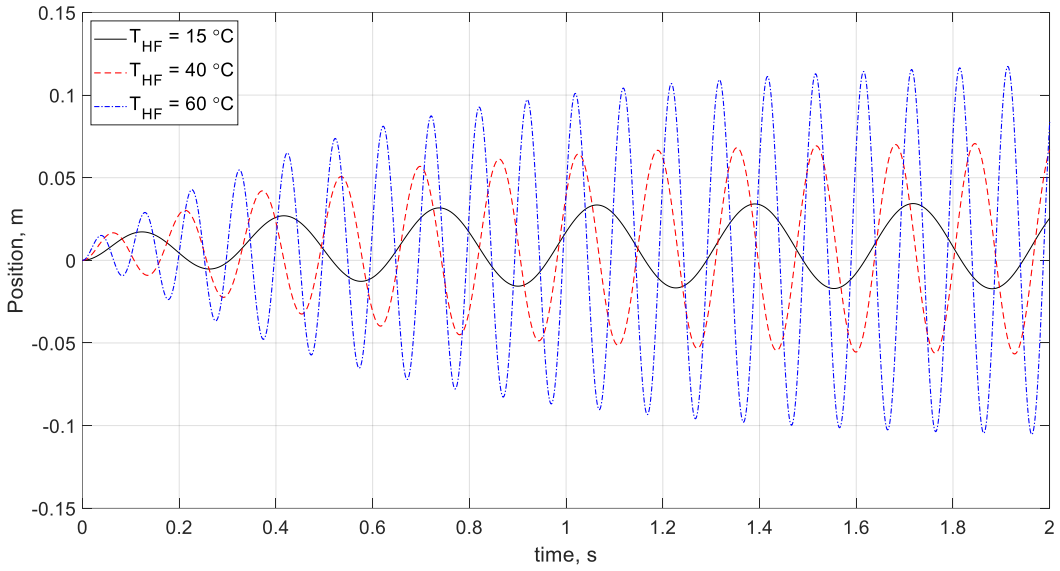

Fig. 2.22 Analytical model showing theoretical oscillating motion for a hybrid fluid of 15% gallium and 85% water in an OHP at different operating temperatures with characteristic length of 107 mm, inner diameter of 2 mm, filling ratio of 50%, and temperature difference of 5 °C

These analytical results show that under different OHP conditions, the analytical models for the hybrid fluid of 15% gallium and 85% water have slightly higher amplitudes but lower oscillation frequencies compared to the analytical models for water. The reason for this is because gallium has a higher dynamic viscosity and density, which affect the oscillating motion equations and therefore models. Furthermore, Fig. 2.23 shows the analytical model comparing the theoretical oscillating motion of water to a hybrid fluid at different volumetric percentages of gallium and water in an OHP.

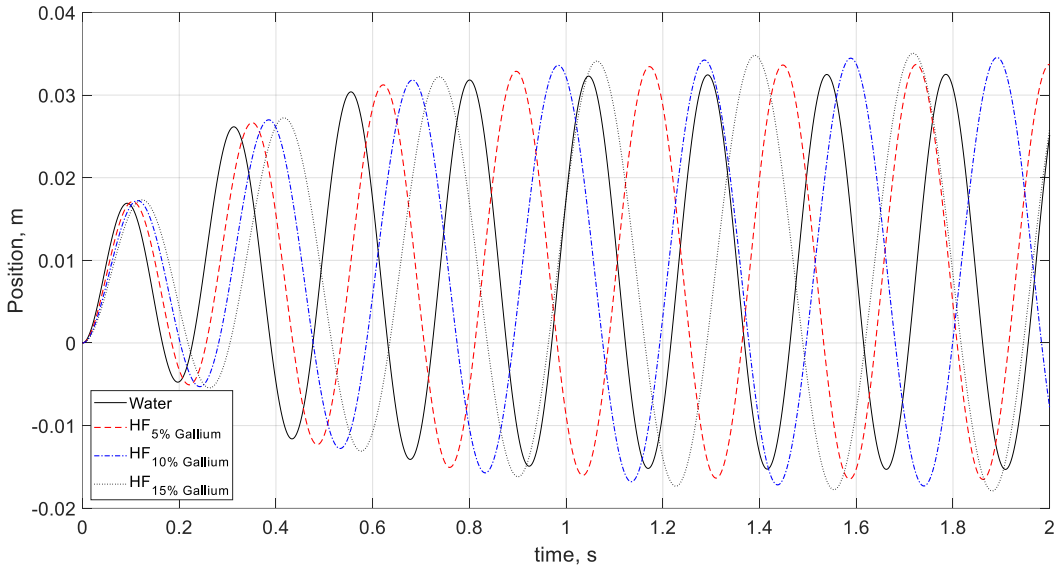

Fig. 2.23 Analytical model comparing the theoretical oscillating motion of water to a hybrid fluid at different volumetric percentages of gallium and water in an OHP with filling ratio of 50%, characteristic length of 107 mm, operating temperature of 15 °C, inner diameter of 2 mm, and maximum temperature difference of 5 °C

Comparing the theoretical oscillating motion of water to a hybrid fluid at different volumetric percentages of gallium and water in an OHP as seen in Fig. 2.23, it becomes apparent that as the volumetric fill ratio of gallium increases (and therefore decreasing the volumetric fill ratio of water), the oscillation frequency decreases while the amplitude increases, and both of these values will have an effect on the heat transfer of the OHP.

Figures 2.24-2.28 show analytical models of the theoretical heat transfer coefficients and temperature differences for water as well as hybrid fluids ranging from 5% to 15% volumetric gallium in the hybrid fluid in an OHP at specified operating conditions.

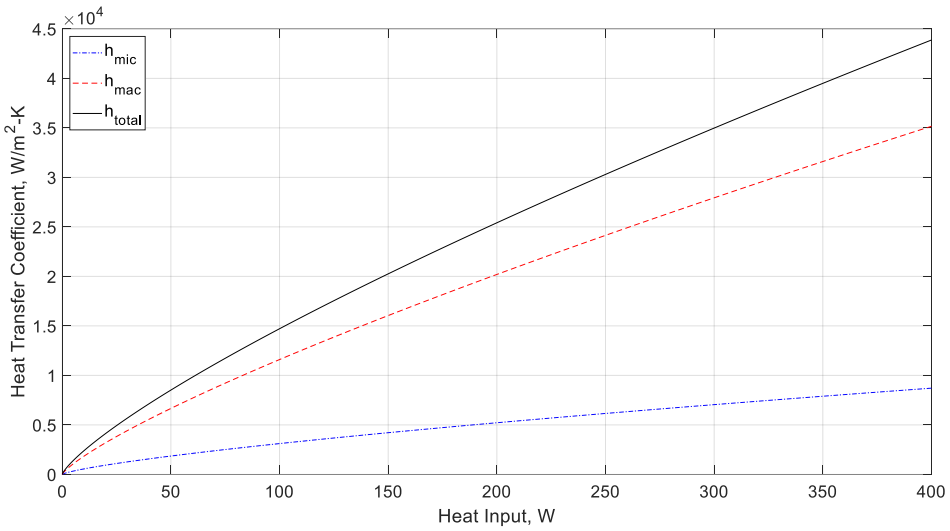

Fig. 2.24 Analytical model showing theoretical macroscopic and microscopic heat transfer coefficients in the evaporating section for water in an OHP with varying power input for an operating temperature of 15 °C, filling ratio of 50%, characteristic length of 107 mm, and inner diameter of 2 mm

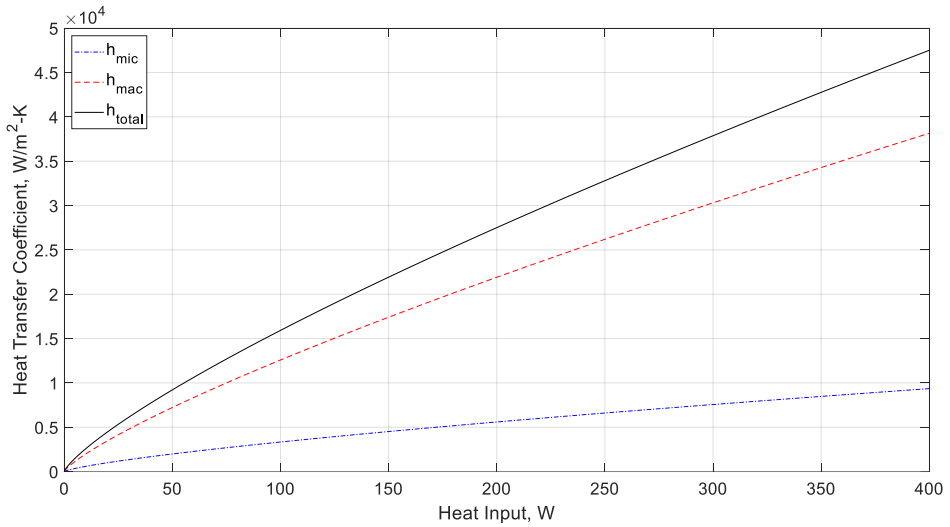

Fig. 2.25 Analytical model showing theoretical macroscopic and microscopic heat transfer coefficients in the evaporating section for a hybrid fluid of 5% gallium and 95% water in an OHP with varying power input for an operating temperature of 15 °C, filling ratio of 50%, characteristic length of 107 mm, and inner diameter of 2 mm

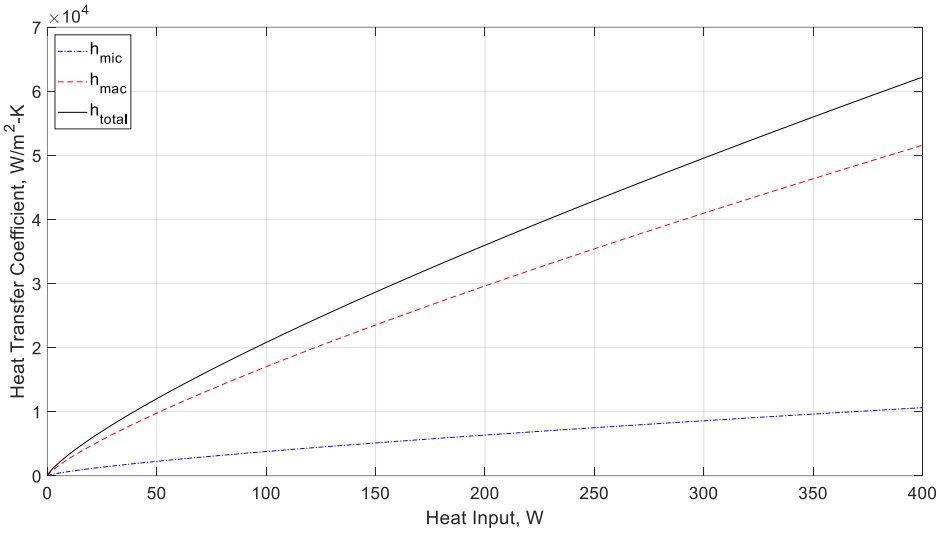

Fig. 2.26 Analytical model showing theoretical macroscopic and microscopic heat transfer coefficients in the evaporating section for a hybrid fluid of 10% gallium and 90% water in an OHP with varying power input for an operating temperature of 15 °C, filling ratio of 50%, characteristic length of 107 mm, and inner diameter of 2 mm

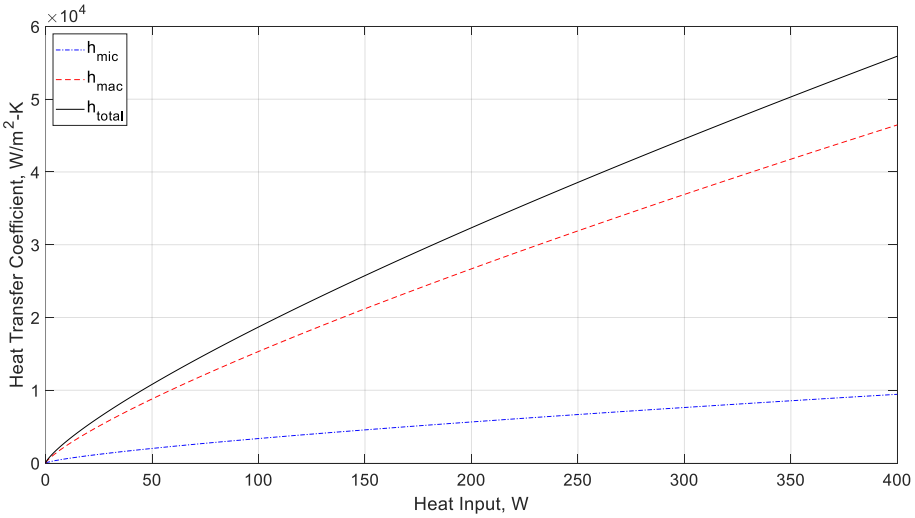

Fig. 2.27 Analytical model showing theoretical macroscopic and microscopic heat transfer coefficients in the evaporating section for a hybrid fluid of 15% gallium and 85% water in an OHP with varying power input for an operating temperature of 15 °C, filling ratio of 50%, characteristic length of 107 mm, and inner diameter of 2 mm

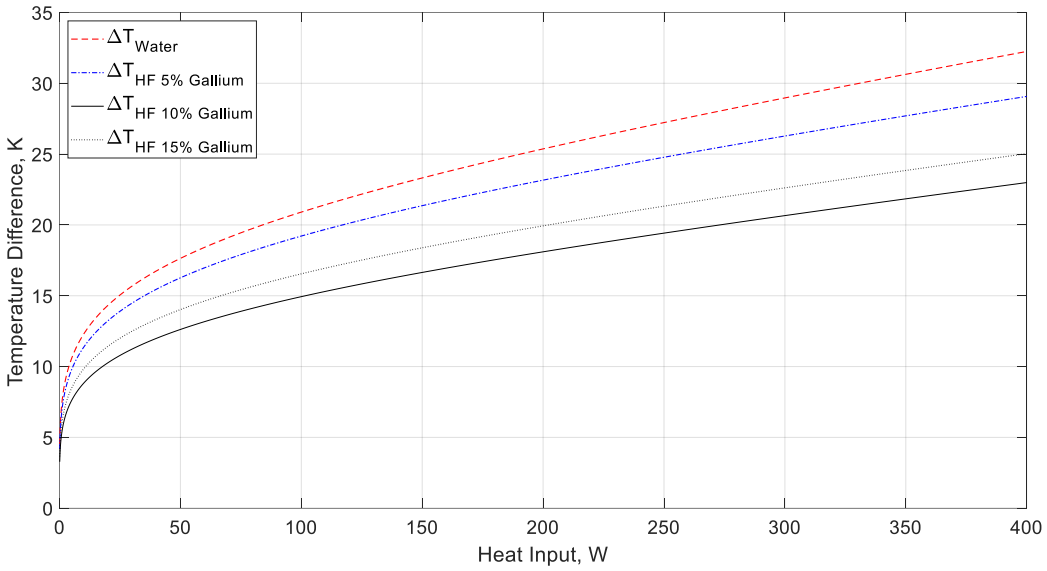

Fig. 2.28 Analytical model showing theoretical temperature differences for water as well as hybrid fluids ranging from 5% to 15% volumetric gallium in the hybrid fluid in an OHP with varying power input at an operating temperature of 15 °C, filling ratio of 50%, characteristic length of 107 mm, and inner diameter of 2 mm

As seen from the results, the microscopic heat transfer contributions that is due to the thin film evaporation is much less than the macroscopic heat transfer due to the forced convection from the oscillating motions. As a result, the heat transfer in the OHP is mainly due to the exchange of sensible heat, which agrees with the results presented by Khandekar et al. [7,8] and Zhang and Faghri [12,13]. The driving force of the oscillating flow is the pressure difference between the condenser and the evaporator. This pressure difference is a result of the phase-change heat transfer occurring in the OHP.

Furthermore, Fig. 2.28 shows that as the volumetric percentage of gallium increases in the hybrid fluid, the heat transfer capabilities also increase, up to a certain point. This is due to the fact that as we increase the volumetric percentage of gallium, the hybrid fluid's dynamic

viscosity, liquid density, liquid thermal conductivity and liquid surface tension increase, while the hybrid fluid's liquid specific heat capacity and overall oscillating motion velocity decrease (due to a minimal increase in amplitude but a lower oscillating frequency between the working fluids as the volumetric percentage of gallium increases). With these effects in mind, one can see that there resides a 'sweet spot' within the equations used that takes advantage of the changes within these mentioned values before losing efficacy.

Chapter III. Experimental Investigation

3.1 Hybrid Fluid Oscillating Heat Pipe Experiment

In order to verify the analytical model predicting the heat transfer performance, experimental investigations were conducted. The experimental system, as shown in Fig. 3.1, consisted of a test section including an OHP, a cooling bath, a power supply, and a data acquisition system.

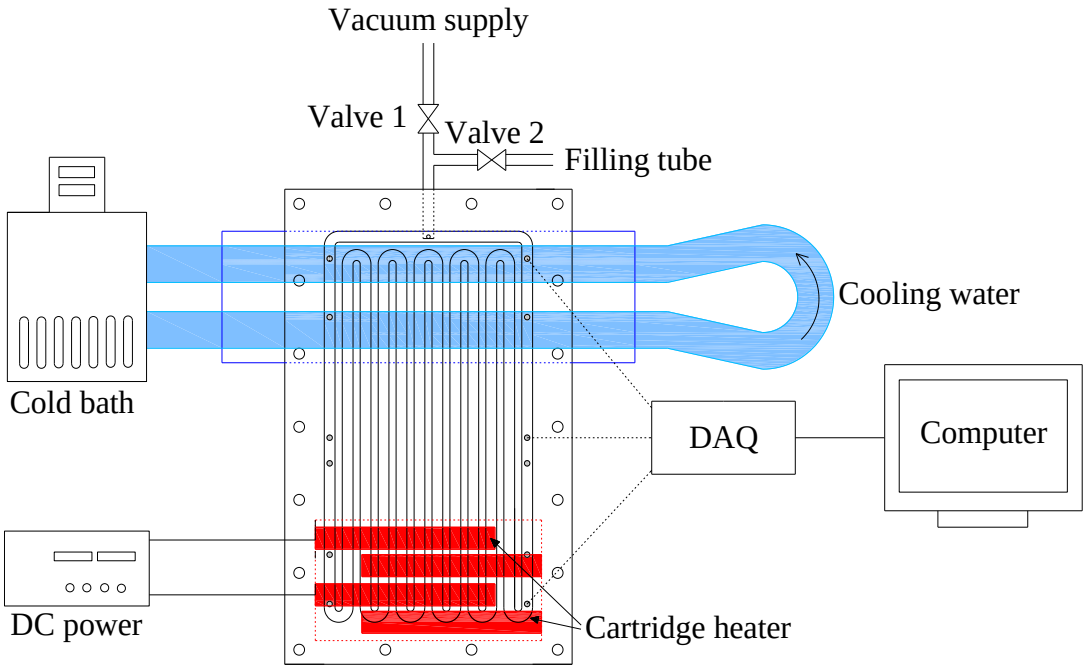

Fig. 3.1 Schematic of experimental OHP system setup

3.1.1 Setup

An OHP with six turns was manufactured on a 130 mm × 80 mm × 10 mm copper plate. The channels (2 × 2 mm^2) were machined into the copper substrate and had six thermocouple ports (with 1.5 mm diameter) drilled on each edge with two in the evaporator, two in the

condenser, and two in the adiabatic section allowing for temperature data collection, as seen in Fig. 3.2.

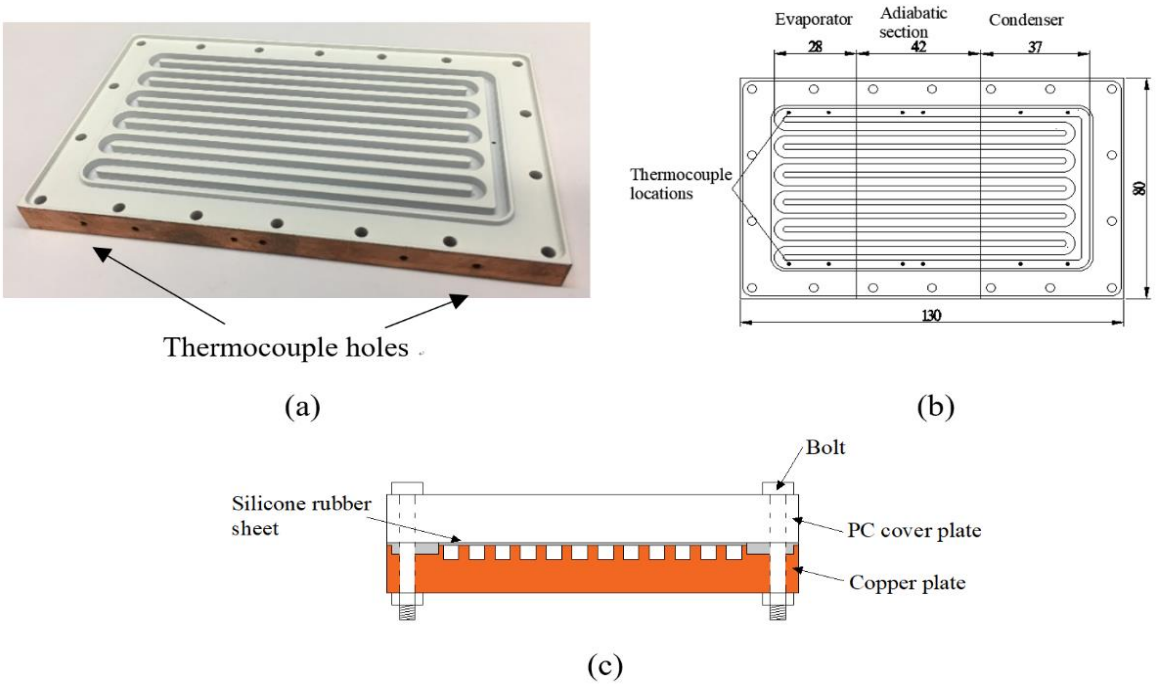

Fig. 3.2 Schematic of OHP used

Furthermore, the copper substrate creates a hydrophobic surface condition and is good at preventing material adherence to the surface. Since the OHPs were to be used for multiple tests, the ability to clean and refill the OHPs was crucial to this experiment. Hydrophobicity is defined by the liquid contact angle with the surface of the OHP greater than 90°. OHPs operate best with a hydrophobic condenser section, since hydrophobic wetting characteristics of liquid metal can significantly enhance the convection heat transfer of oscillating flow from the evaporator to condenser through the high thermal conductivity of liquid metal, reduction of the pressure drop, and condensation heat transfer in cavities. OHPs operate best with a hydrophilic evaporative section, since the hydrophilic wetting characteristics can enhance thin film evaporation [27], which significantly increases the driving force for the oscillating motion. The microchannels

were then sealed with two translucent silicone rubber sheets and gasket to prevent gas or liquid leakage at a high-pressure difference between ambient and internal. A translucent acrylic plate was then bolted to the OHP, leaving the channels visible through the plate as shown in Fig. 3.3.

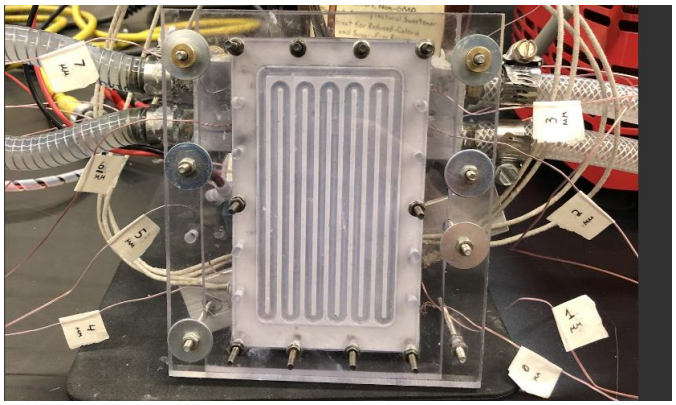

Fig. 3.3 Picture showing the visible channels through the clear plate

To emulate a heat source, a 63 mm x 33 mm copper heater block with four internally placed cartridge heaters was attached to the lower portion of the OHP backside and was centered horizontally on the back of the OHP splitting the distance equally between the four 12.7 mm deep thermocouple ports. The heater block was attached to the copper OHP using a thin film of Omegatherm 201 silicon thermal grease in order to reduce contact resistance to the copper. By equally centering the heater block over the four thermocouple ports, the evaporator section can then have a spatially averaged temperature for higher accuracy than measuring with a single thermocouple. A 115 mm × 38 mm aluminum cooling block was also attached using a thin film of Omegatherm 201 silicon thermal grease with a two-pass heat exchanger pumping water on the opposite end from the evaporator. The cooling block was centered to have the two thermocouple locations measuring the condenser temperatures equally divided into halves for accurate temperature averaging. The OHP experimental setup can be seen in Fig. 3.4.

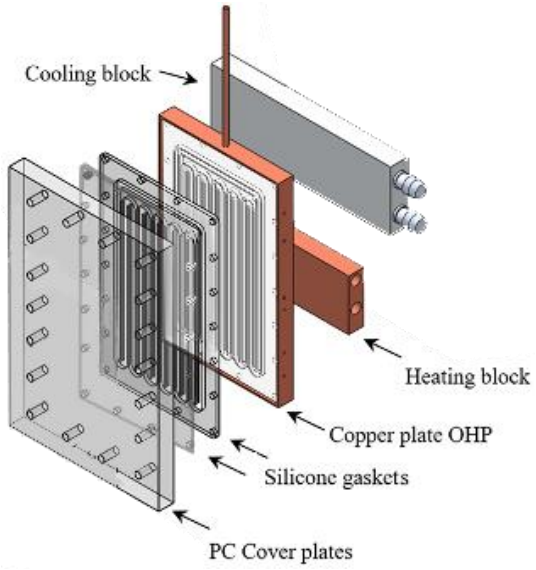

Fig. 3.4 Schematic of the OHP experimental setup

The two blocks were fastened to the OHP with thin wire to ensure all heat dissipation occurred through the working fluid, not the fasteners. The entire assembly was thermally isolated using fiberglass insulation and low emissivity foil coated bubble wrap to reduce the heat loss, as shown in Fig. 3.5.

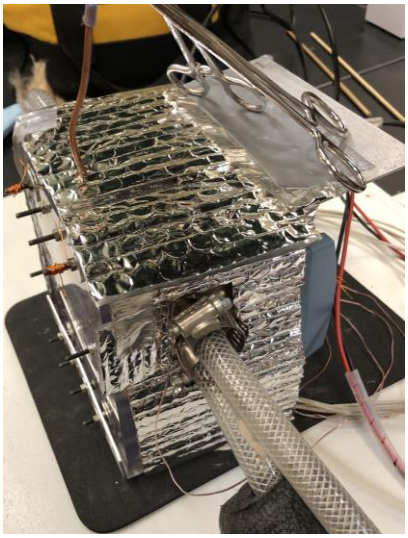

Fig. 3.5 Picture showing the thermal insulation around the OHP experimental setup

3.1.2 Filling the Hybrid Fluid Oscillating Heat Pipe

In order to fill the OHP with the hybrid fluid, the OHP underwent a backfilling process to evacuate all of the air within the channels. This process involved attaching the charge tube, shown in Fig. 3.5, to a vacuum pump with surgical tubing to decrease the internal pressure to approximately 30 Pa then filling the assembly completely with distilled water. The water is then pumped out and evaporated using the vacuum pump. This process was repeated twice in order to ensure no air remains and any residual pressure is water vapor. The hybrid fluid was premeasured using the OHAUS Explorer EX1103 balance. The hybrid fluid was then filled to 40%, 50%, and 60% of the internal channel volume. Prior to removing the vacuum pump tubing from the OHP charge tube, the vacuum tubing was clamped to prevent pressure equalization. A third tubing line sealed until this point connecting to the OHP was attached to the measured hybrid fluid in a glass syringe. Upon releasing the sealing clamp on the third line, the pressure difference forces the hybrid fluid into the OHP. The rate of fill was controlled by slowly releasing the syringe plunger while measuring the change in mass of the total assembly to gage the actual fill mass.

3.1.3 Data Acquisition

Prior to the start of the experiment, the system was allowed to equilibrate and reach steady state such that the steady-state operating temperature was achieved and a uniform temperature distribution with no heater power input was observed throughout the HFOHP. Once the experimental system reached the equilibrium, the input power was increased in 50 W increments up to a maximum heat input of 400 W. The steady-state condition was defined as the mean temperature in the evaporator with a change of less than 0.5°C in 5 min.

The control test was conducted using distilled water only as the working fluid. The data collected was utilized as a benchmark for comparing the hybrid fluids. Data was collected using 16 channel 24-Bit multifunction MC USB-2408 Series temperature and voltage data acquisition measurement (DAQ) device with eight type T thermocouples. All thermocouples were calibrated with the maximum uncertainty of ± 0.05°C. Temperature data was collected using the DAQ to measure the temperatures from the locations denoted in Fig. 3.3. The four thermocouples in the evaporator section had their data spatially averaged to have a single value denoting the average temperature of the evaporator with higher accuracy. The two thermocouples measuring the condenser section were spatially averaged to have a single value denoting the average temperature of the condenser. Subtracting the condenser temperature from the evaporator temperature yielded the average temperature difference for each HFOHP test with the hybrid fluid at the specific power inputs after thermal equilibrium was reached. After the experimental setup reached 400 W and had reached thermal equilibrium, the power was removed, and data collection was kept on to capture the equalization rate of the test OHP.

The maximum output voltage and current of the N5750A DC power is 150 ± 0.15 V and 5 ± 0.015 A. The relative uncertainty of the input power is calculated by

$$\frac{\delta Q}{Q} = \sqrt{\left(\frac{\delta V}{V}\right)^2 + \left(\frac{\delta I}{I}\right)^2} \tag{3.1.1}$$

The relative uncertainty of thermal resistance is determined by

$$\frac{\delta R}{R} = \sqrt{\left(\frac{\delta T_e}{T_H - T_C}\right)^2 + \left(\frac{\delta T_C}{T_H - T_C}\right)^2 + \left(\frac{\delta Q}{Q}\right)^2} \tag{3.1.2}$$

At the heat input of 50-400 W, the temperature difference between the condenser and the evaporator is 10.2-32.3 ℃. The relative uncertainty of the input power is 0.31%-0.52%. The

relative uncertainty of the thermal resistance is 1.62%-3.73%.

3.1.4 Results and Discussion

The temperatures of the evaporator and condenser measured during the HFOHP experiments were measured, and they were recorded by the stabilized temperature at the end of each power step. Subtracting the averaged condenser temperature from the averaged evaporator temperature yielded the average temperature difference for each OHP experiment at each power input step after thermal equilibrium was reached. The temperature difference results between the averaged evaporator and condenser temperatures at every power input step are shown in Tables 3.1-3.3.

Table 3.1 Average temperature differences between evaporator and condenser at 40% fill ratio

Power [W]	Water	Hybrid Fluid (5% Gallium and 95% Water)	Hybrid Fluid (10% Gallium and 90% Water)	Hybrid Fluid (15% Gallium and 85% Water)
50	10.66955	11.5613	11.17375	11.5528
100	14.92537	17.24138	13.29695	14.3572
150	20.00514	20.00917	15.0566	15.1215
200	21.05263	20.01629	14.4271	16.6728
250	22.72727	21.73913	15.89875	19.3734
300	25.01845	23.07692	16.3367	18.73175
350	26.92308	24.13793	17.7581	20.57025
400	28.57143	26.0933	19.63865	22.98851

Table 3.2 Average temperature differences between evaporator and condenser at 50% fill ratio

Power [W]	Water	Hybrid Fluid (5% Gallium and 95% Water)	Hybrid Fluid (10% Gallium and 90% Water)	Hybrid Fluid (15% Gallium and 85% Water)
50	10.20408	10.9425	11.24455	11.19065
100	17.24138	19.60325	18.18182	18.86792
150	20.54795	20.83333	21.42857	21.12676
200	22.47191	21.05263	17.3913	18.6151
250	27.77778	25.00815	17.85714	19.12365
300	28.88905	27.27273	20.00382	21.7676
350	29.33397	26.92308	21.21212	22.37515
400	32.35526	28.98255	23.2868	24.3542

Table 3.3 Average temperature differences between evaporator and condenser at 60% fill ratio

Power [W]	Water	Hybrid Fluid (5% Gallium and 95% Water)	Hybrid Fluid (10% Gallium and 90% Water)	Hybrid Fluid (15% Gallium and 85% Water)
50	12.16955	12.51741	12.75016	13.02514
100	18.00382	19.00195	18.00482	20.00693
150	21.01839	24.01852	22.57502	25.05024
200	24.00581	26.00981	26.00914	28.00593
250	27.51124	26.75042	26.25019	27.50153
300	30.01069	28.51052	25.50026	27.90415
350	31.6751	29.75005	25.90195	28.3595
400	36.00671	33.60329	26.8896	31.00025

These experimental results were plotted against the theoretical results found earlier and can be seen in Figs. 3.6-3.8.

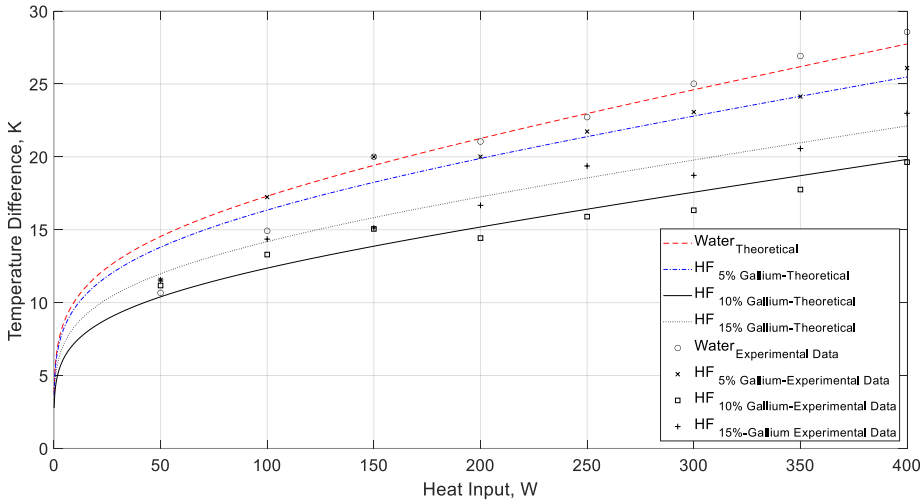

Fig. 3.6 Plot showing theoretical and experimental temperature differences for water as well as hybrid fluids ranging from 5% to 15% volumetric gallium in the hybrid fluid in an OHP with varying power input at an operating temperature of 15 °C, filling ratio of 40%, characteristic length of 107 mm, and inner diameter of 2 mm

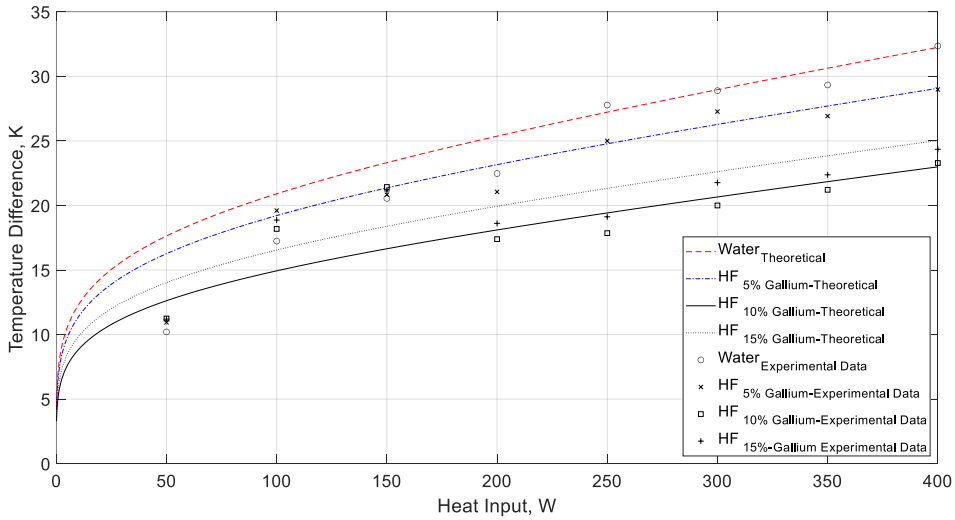

Fig. 3.7 Plot showing theoretical and experimental temperature differences for water as well as hybrid fluids ranging from 5% to 15% volumetric gallium in the hybrid fluid in an OHP with varying power input at an operating temperature of 15 °C, filling ratio of 50%, characteristic length of 107 mm, and inner diameter of 2 mm

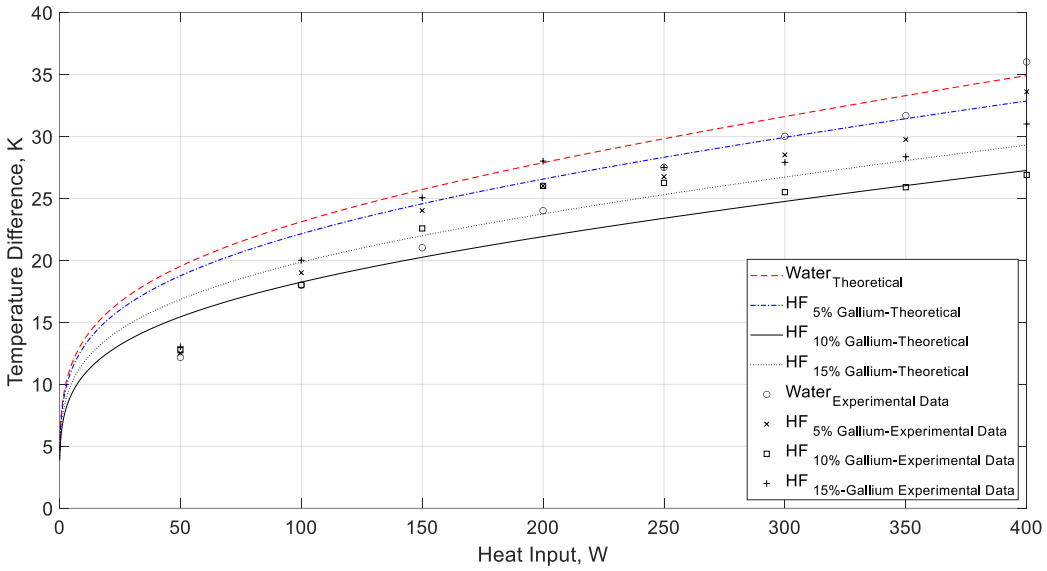

Fig. 3.8 Plot showing theoretical and experimental temperature differences for water as well as hybrid fluids ranging from 5% to 15% volumetric gallium in the hybrid fluid in an OHP with varying power input at an operating temperature of 15 °C, filling ratio of 60%, characteristic length of 107 mm, and inner diameter of 2 mm

As one can see from the graphs, the theoretical results compared to the experimental results are not very precise at low power inputs, but that discrepancy greatly decreases as the power input increases and the theoretical and experimental results become a lot more agreeable with one another. Considering that the pressure drops in the turns of the OHP and possible circulation of working fluid were not taken into account in the theoretical model, the discrepancy between the theoretical and experimental results are reasonable. Another thing to note is that the discrepancy between the theoretical results and the experimental results also increased as the total filling ratio increased from 40% to 60%. This is due to the fact that the theoretical results are based on the assumption that oscillatory motion starts as soon as heat input begins, which is certainly not the case in real-life applications. Yin et al. [34] studied the effects of heat input

needed to start the oscillating motion in an OHP depending on the filling ratio. It was noticed that when the filling ratio increases, the heat input required to start up the oscillating motion increases; furthermore, there exists an upper limit. This upper limit of the filling ratio is dependent on the properties of the working fluid.

Although the theoretical results are not 100% accurate, it provides a good indication of how the OHP might perform with given parameters, which can help save time in experimental setups and help figure out which parameters might perform the best, allowing us to run physical experiments on them at a faster rate.

From the raw temperature data, further analysis was conducted in order to find the thermal resistance of the HFOHP using the relation:

$$R = \frac{\Delta T}{Q} \tag{3.1.3}$$

Once the thermal resistance was calculated, the thermal conductance could then be solved for by the relation:

$$C = \frac{1}{R} \tag{3.1.4}$$

Figures 3.9-3.11 show the thermal conductance of water as well as the different hybrid fluid ratios used in the HFOHP.

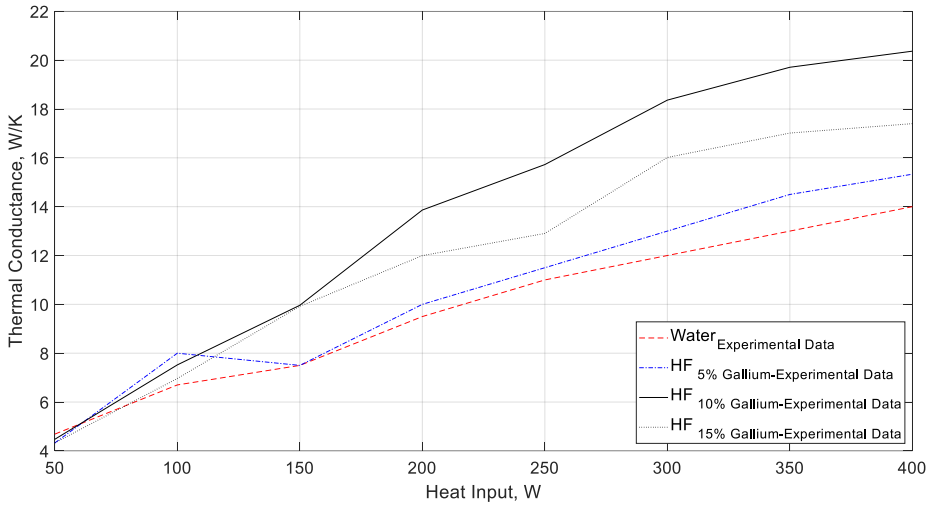

Fig. 3.9 Graph showing the thermal conductance for water as well as hybrid fluids ranging from 5% to 15% volumetric gallium in the hybrid fluid in an OHP with varying power input at an operating temperature of 15 °C, filling ratio of 40%, characteristic length of 107 mm, and inner diameter of 2 mm

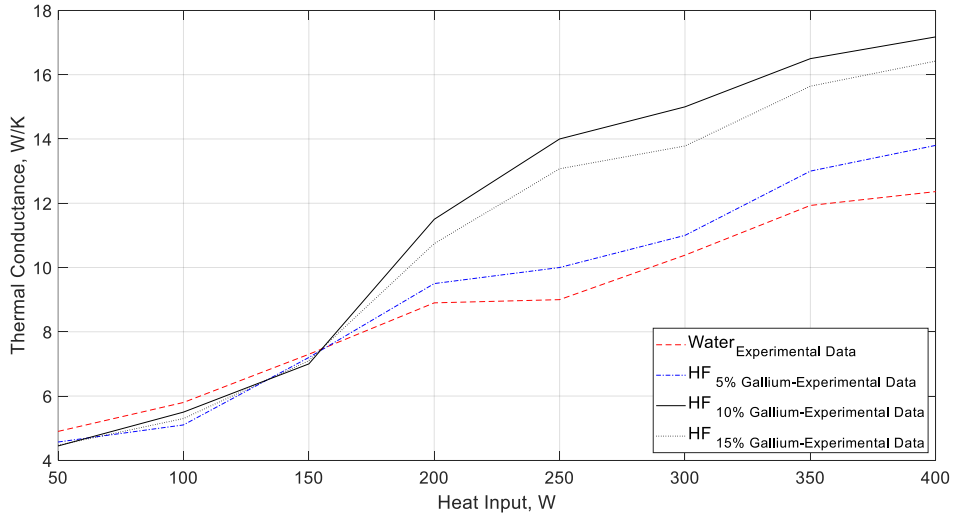

Fig. 3.10 Graph showing the thermal conductance for water as well as hybrid fluids ranging from 5% to 15% volumetric gallium in the hybrid fluid in an OHP with varying power input at an operating temperature of 15 °C, filling ratio of 50%, characteristic length of 107 mm, and inner diameter of 2 mm

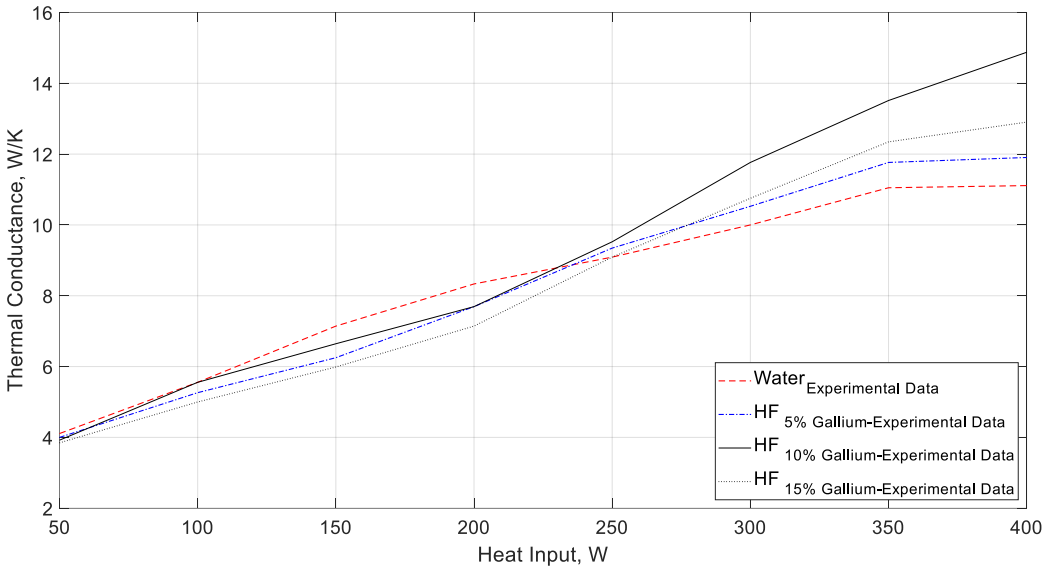

Fig. 3.11 Graph showing the thermal conductance for water as well as hybrid fluids ranging from 5% to 15% volumetric gallium in the hybrid fluid in an OHP with varying power input at an operating temperature of 15 °C, filling ratio of 60%, characteristic length of 107 mm, and inner diameter of 2 mm

From Figs. 3.9-3.11, one can see around what power input the HFOHP began its oscillatory motion. It was noticed that as the filling ratio increased, the heat input required to start up the oscillating motion increased as well. In terms of best performance, it boiled down to two factors. The first factor was the total filling ratio. Based on the experimental data gathered as well as the theoretical models plotted, it was observed that as the total filling ratio decreased (from 60% to 40%), the thermal conductance of the working fluid increased, regardless of the working fluid inside the OHP. The second factor was the hybrid fluid ratio. Based on the experimental data gathered as well as the theoretical models plotted, it was observed that the hybrid fluid of gallium and water performed better than pure water, regardless of the volumetric ratio of gallium in the OHP. With that being said, it is observed that there exists a ‘sweet spot’

within the hybrid fluid ratio that performs the best. With the experiments conducted in this research, it was observed that a 10% volumetric ratio of gallium within the hybrid fluid performed the best, regardless of the total filling ratio. This is due to the fact that as the volumetric ratio of gallium increases within the hybrid fluid, there are a number of variables that change value, including the thermal properties as well as the overall velocity of the hybrid fluid. It was observed that at a certain point, when volumetric gallium percentage is increased, the increase in thermal conductivity loses its efficacy since the hybrid fluid's velocity also decreases and therefore reduces the amount of forced convective heat transfer able to be produced that the gallium's effective heat transfer relies heavily on. With all this being said, it was observed that the hybrid fluid of 10% gallium and 90% water with a total fill ratio of 40% performed the best with the given OHP parameters.

Chapter IV. Conclusions

A study of the effects of hybrid fluids in an oscillating heat pipe was conducted both analytically and experimentally to determine whether HFOHPs are viable for applications in high-powered systems. Mathematical models predicting the oscillatory motions as well as the heat transfer effects of hybrid fluids in an oscillating heat pipe were developed analytically and simulated through MATLAB. These analytical models included the forced convection heat transfer as a result of the oscillating motions, the thin film evaporation heat transfer, as well as the thin film condensation heat transfer. Results show that although the HFOHPs produced less overall oscillating motions compared to a water OHP, it produced an enhancement in heat transfer and therefore a decreased temperature difference between the evaporator and condenser during operation compared to a water OHP because of the change in various thermal properties. Within these HFOHP experiments, it was observed that there exists a 'sweet spot' of volumetric ratio of gallium within the hybrid fluid that performed the best, and this was due to the fact that it had the best heat transfer capability in terms of the change in thermal properties while not being heavily governed by the decrease in its overall oscillatory velocity. This investigation also found that the experimental investigation results resemble and follow the same trends as the analytical simulations. It can be concluded that when the OHP is charged with a hybrid fluid involving a liquid metal, the heat transfer capabilities can be enhanced in high-powered systems. These results can help advance current cooling capabilities and limitations, and the technology can be readily used in many fields such as naval GBIT devices, aerospace lightweight heat spreaders, satellite cooling systems, solar energy, HVAC, power plants, and heat exchangers.

References

[1] Akachi, H., 1990, "Structure of a Heat Pipe," U.S. Patent No. 4,921,041.

[2] Ma, H. B., Wilson, C., Yu, Q., Choi, U. S., and Tirumala, M., 2006, "An Experimental Investigation of Heat Transport Capability in a Nanofluid Oscillating Heat Pipe," ASME J. Heat Transfer, 128, pp. 1213–1216.

[3] Zhang, X. M., Xu, J. L., and Zhou, Z. Q., 2004, "Experimental Study of a Pulsating Heat Pipe Using FC-72, Ethanol, and Water as Working Fluids," Exp. Heat Transfer, 17, pp. 47–67.

[4] Park, K., and Ma, H. B., 2007, "Nanofluid Effect on the Heat Transport Capability in a Well-Balanced Oscillating Heat Pipe," J. Thermophys. Heat Transfer, 21(2), pp. 443–445.

[5] Kim, J. H., Lee, W. H., Jung, H. S., and Kim, J. S., 2000, "Characteristics of Pressure Oscillation in Self-Excited Oscillating Heat Pipe Based on Experimental Study," *Sixth International Heat Pipe Symposium,* Chiang Mai, Thailand, pp. 263–272.

[6] Borgmeyer, B., and Ma, H. B., 2007, "Experimental Investigation of Oscillating Motions in a Flat Plate Pulsating Heat Pipe," J. Thermophys. Heat Transfer, 21(2), pp. 405–409.

[7] Khandekar, S., and Groll, M., 2003, "An Insight into Thermo-Hydrodynamic Coupling in Closed Loop Heat Pipes," Int. J. Therm. Sci., 43(1), pp. 13–20.

[8] Khandekar, S., Nanyam, S., and Groll, M., 2004, "Two-Phase Flow Modeling in Closed Loop Pulsating Heat Pipes," *13th International Heat Pipe Conference,* Sept. 19–25.

[9] Zuo, J., North, M. T., and Wert, K. L., 2001, "High Heat Flux Heat Pipe Mechanism for Cooling of Electronics," IEEE Trans. Compon. Packag. Technol., 24(2), pp. 220–225.

[10] Lin, L., Ponnappan, R., and Leland, J., 2001, "Experimental Investigation of Oscillating Heat Pipes," J. Thermophys. Heat Transfer, 15(4), pp. 395–400.

[11] Qu, W., and Ma, H. B., 2007, “Theoretical Analysis of Start-up of a Pulsating Heat Pipe,” Int. J. Heat Mass Transfer, 50, pp. 2309–2316.

[12] Zhang, Y., and Faghri, A., 2003, “Oscillatory Flow in Pulsating Heat Pipes with Arbitrary Numbers of Turns,” J. Thermophys. Heat Transfer, 17(3), pp. 340–347.

[13] Zhang, Y., and Faghri, A., 2002, “Heat Transfer in an Oscillating Heat Pipe with Open End,” Int. J. Heat Mass Transfer, 45(4), pp. 755–764.

[14] Ma, H. B., Hanlon, M. A., and Chen, C. L., 2006, “An Investigation of Oscillating Motions in a Miniature Pulsating Heat Pipe,” Microfluid. Nanofluid., 2(2), pp. 171–179.

[15] Wong, T. N., Tong, B. Y., Lim, S. M., and Ooi, K. T., 1999, “Theoretical Modeling of Oscillating Heat Pipe,” *Proceedings of 11th International Heat Pipe Conference*, Tokyo, Japan, pp. 159–163.

[16] Ma, H. B., Borgmeyer, B., Cheng, P., and Zhang, Y. (May 29, 2008). "Heat Transport Capability in an Oscillating Heat Pipe." ASME. J. Heat Transfer. August 2008; 130(8): 081501.

[17] Ma, K., and Liu, J., 2007, “Liquid metal cooling in thermal management of computer chips,” Front. Energy Power Eng. China, 1, pp. 384–402.

[18] Chen, J. C., 1966, “Correlation for Boiling Heat Transfer to Saturated Fluids in Convective Flow,” Ind. Eng. Chem. Process Des. Dev., 5(3), pp. 322–339.

[19] Zhao, T. S., and Cheng, P., 1998, “Heat Transfer in Oscillatory Flows,” *Annual Review of Heat Transfer*, C. L. Tien, ed., Begell House, Inc., Redding, CT, Vol. IX, No. 9, pp. 359–420.

[20] Wallis, G. B., 1969, *One-Dimensional Two-Phase Flow*, McGraw-Hill Book Company, New York.

[21] Peterson, G. P., 1994, *An Introduction to Heat Pipe: Modeling, Testing, and Applications*, Wiley, New York.

[22] Yuan, H., Oguz, H. N., and Prosperetti, A., 1999, "Growth and Collapse of a Vapor Bubble in a Small Tube," Int. J. Heat Mass Transfer, 42(19), pp. 3643–3657.

[23] Thomas, K. J., and Kim, C. J., 1998, "Valveless Pumping Using Traversing Vapor Bubbles in Microchannels," J. Appl. Phys., 83(11), pp. 5658–5664.

[24] Kurzweg, U. H., 1985, "Enhanced Heat Conduction in Fluids Subjected to Sinusoidal Oscillations," ASME J. Heat Transfer, 107(3), pp. 459–462.

[25] Kurzweg, U. H., and Zhao, L. D., 1984, "Heat Transfer by High-Frequency Oscillations: A New Hydrodynamic Technique for Achieving Large Effective Thermal Conductivities," Phys. Fluids, 27(11), pp. 2624–2627.

[26] Hao, T., Ma, H., and Ma, X., 2019, "Experimental Investigation of Oscillating Heat Pipe With Hybrid Fluids of Liquid Metal and Water," ASME. J. Heat Transfer, 141(7), 071802.

[27] Lam, L., Hodes, M., and Enright, R., 2015, "Analysis of Galinstan-Based Microgap Cooling Enhancement Using Structured Surfaces," J. Heat Transfer, 137.

[28] Enright, R., Hodes, M., Salamon, T., and Muzychka, Y., 2013, "Isoflux Nusselt Number and Slip Length Formulae for Superhydrophobic Microchannels," J. Heat Transfer, 136.

[29] Ng, C.-O., and Wang, C. Y., 2009, "Stokes shear flow over a grating: implications for superhydrophobic slip," Phys. Fluids, 21, 013602.

[30] Ybert, C., Barentin, C., Cottin-Bizonne, C., Joseph, P., and Bocquet, L., 2007, "Achieving large slip with superhydrophobic surfaces: Scaling laws for generic geometries," Phys. Fluids, 19, 123601.

[31] Rothstein, J. P., 2010, “Slip on superhydrophobic surfaces,” Annu. Rev. Fluid Mech., 42, pp. 89–109.

[32] Kendall, J., Monroe, K. P., and Amer, J., 1917, Chem. Soc., 39, pp. 1787.

[33] Jamieson, D. T., and Irving, J. B., 1974, "Thermal conductivity of binary liquid mixtures," TNA Kew.

[34] Yin, D., Rajab, H., and Ma, H.B., 2014, “Theoretical analysis of maximum filling ratio in an oscillating heat pipe,” Int. J. Heat Mass Transfer, 74, pp. 353-357.

[35] Xu, Q., Oudalov, N., Guo, Q., Jaeger, H., M., and Brown, B., 2012, “Effect of oxidation on the mechanical properties of liquid gallium and eutectic gallium-indium,” Phys. Fluids, 24(6), pp. 123-141.

[36] Vignarooban, K., Xu, X., Arvay, A., Hsu, K., and Kannan, A., 2015, “Heat transfer fluids for concentrating solar power systems – A review,” Applied Energy, 146.

[37] Sen, P., and Kim, C., 2009, “A Fast Liquid Metal Droplet Microswitch Using EWOD-Driven Contact-Line Sliding,” J. Microelectromechanical Systems, 18(1), pp. 174-185.

[38] Aviles, A., and Merwin, M. R., 2018, “Erythritol solubility increase with thermal energy input effect on density and viscous flow in a closed system.”

[39] Ma, H. B., 2015, *Oscillating Heat Pipes*, Springer New York.